PALEOCEANOGRAPHY, VOL. 6, NO. 4, PAGES 395-430, AUGUST 1991

GLACIAL pCO_2 REDUCTION BY THE WORLD OCEAN: EXPERIMENTS WITH THE HAMBURG CARBON CYCLE MODEL

C. Heinze[1] and E. Maier-Reimer

Max-Planck-Institut für Meteorologie,
Hamburg, Federal Republic of Germany

K. Winn

Geologisch-Paläontologisches Institut und
Museum der Christian-Albrechts-Universität,
Kiel, Federal Republic of Germany

Abstract. Possible mechanisms for the 80 ppm reduction of atmospheric CO_2 partial pressure during the last glaciation were investigated using the Hamburg Ocean Carbon Cycle Model. The three-dimensional carbon cycle model is based on the velocity field of the Hamburg Large-Scale Geostrophic Ocean General Circulation Model and uses the same grid as that model. The horizontal resolution (3.5° x 3.5°) is lower than the length scale of narrow upwelling belts which could not be represented adequately in this study, but the large-scale features of the ocean carbon cycle are reproduced rather well. Sensitivity experiments were carried out to investigate the role of chemical and biological parameters (nutrient cycling, composition of biogenic particulate matter, CO_2 solubility) and different circulation regimes for the atmospheric CO_2 content. The model responses were compared to deep-sea sediment core records and ice core data from the last glaciation. Each experiment was compared with observed average tracer patterns during 18–65 kyr B.P. It was found that none of the sensitivity experiments alone could explain all observed tracer changes (atmospheric pCO_2, $\Delta\delta^{13}C_{planktonic-benthic}$, $\delta^{13}C_{benthic}$ differences, $CaCO_3$ corrosivity indices) simultaneously, even in a qualitative sense. Thus according to the model none of the scenarios tested proves to be completely acceptable. The residual discrepancies between the observed and modeled tracer records can probably be attributed to the as yet inadequate reconstruction of the glacial ocean circulation. It is therefore suggested that more effort should be devoted to realistically reproducing the ice age ocean circulation field making use of the forthcoming glacial radiocarbon data base. The residuals between the realistically modeled and observed carbon cycle tracers ($\delta^{13}C$, $CaCO_3$ saturation) should then reveal more clearly the real cause for the observed pCO_2 decrease in the glacial atmosphere.

1. INTRODUCTION

Measurements of CO_2 enclosed in air bubbles of Arctic and Antarctic ice sheets provide evidence for a reduction of atmospheric CO_2 partial pressure (pCO_2) during the last glaciation [e.g., Delmas et al., 1980; Neftel et al., 1982; Oeschger et al., 1985]. The Antarctic Vostok

[1]Now at Institut für Meereskunde der Universität Hamburg, Hamburg, Federal Republic of Germany.

Paper number 91PA00489.
0883-8305/91/91PA-00489$10.00

ice core pCO_2 curve [Barnola et al., 1987] covering the last 160,000 years reveals pCO_2 values near 300 ppm at the last interglacial at about 130 kyr B.P. (kyr B.P. = 10^3 years before present), a decrease to about 200 ppm at the last glacial maximum (about 18 kyr B.P.), and a sharp postglacial increase toward the preindustrial level around 280 ppm. The corresponding local Antarctic air temperature record (obtained from deuterium measurements [Jouzel et al., 1987]) parallels the pCO_2 record, with a maximum glacial-interglacial amplitude of about 12 K.

Small changes in the oceanic carbon cycle have generally been favored as an explanation for Quaternary pCO_2 variations in the atmosphere, because the ocean is the largest quickly recycling carbon pool in direct exchange with the atmospheric reservoir (ocean:atmosphere carbon pool size ratio $\approx$ 60:1; turnover time scales in different oceanic regimes from upper waters to bottom waters: 1–1000 years).

To test some of the hypotheses which have been proposed to explain the observed atmospheric pCO_2 variations, we present in this paper a suite of sensitivity studies with a global high-resolution carbon cycle model based on the velocity field of an ocean general circulation model (OGCM). The experiments focus on the chemical, biological, and physical parameters of the ocean carbon cycle that affect the atmospheric CO_2 partial pressure. The results of these experiments are considered relative to a control run. The deviations are compared with paleoclimate data derived from ice core and sediment core records.

Previous glacial ocean modeling studies have mostly been based on low-resolution kinematic box models [e.g., Knox and McElroy, 1984; Sarmiento and Toggweiler, 1984; Siegenthaler and Wenk, 1984; Broecker and Peng, 1987a; Boyle, 1988]. Box models enable many experiments to be carried out with modest computer resources. They are limited, however, by low horizontal and vertical resolution and the lack of a detailed velocity field constrained by fluid dynamics.

The Hamburg Carbon Cycle Model applied here is based on the velocity field of the dynamical Hamburg Large-Scale Geostrophic OGCM. Although this model is of course still a simplification of the real ocean, many of the basic disadvantages of purely kinematic models no longer occur. The model reproduces the complex three-dimensional structures of water mass properties rather than only basin-wide mean values for a certain depth range. The velocity field is sufficiently realistic to provide the basis for the simulation of chemical interactions and tracer distributions, which depend critically on the oceanic circulation. Sensitivity studies with the high-resolution model can take into account the complexity of the real ocean, thereby allowing a more reliable quantitative interpretation. Model results can be directly compared with observed patterns of water mass properties and geological data as derived from sediment core analyses (which are often valid only for a restricted region with special hydrographic conditions). Furthermore, different kinds of surface forcing can be applied in the dynamical OGCM that defines the velocity field, providing the opportunity to develop physically consistent oceanic circulation patterns under different meteorological and hydrological boundary conditions. The price for these advantages, apart from the higher computer costs, is that a complex model is generally more difficult to interpret than a simpler box model (cause-effect links may be less obvious).

Three different oceanic carbon pumps influence the atmospheric CO_2 partial pressure via the air-sea-gas exchange (Figure 1):

1. The solubility of CO_2 gas in sea-water rises with decreasing temperature and salinity [Weiss, 1974]. Cold and low-salinity water can store more carbon than warm or highly haline water. Thus a cooling or freshening of the surface water effects a reduction of the atmospheric CO_2 partial pressure.

2. Carbon and biolimiting nutrients are extracted from surface waters by planktonic biota for the production of organic carbon soft tissue (particulate organic carbon, POC). The stronger the production of this biogenic particulate organic carbon, the lower the CO_2 partial pressure within the surface waters and in the overlying air ("biological pump").

3. Besides organic soft tissue, planktonic biota produce hard parts (shell material) of either opaline (SiO_4) or calcareous ($CaCO_3$) material. SiO_4 production and dissolution do not directly influence the carbon cycle. Production of $CaCO_3$, however, leads to a decrease of alkalinity by extraction of CO_3^{2-} ions from the water column,

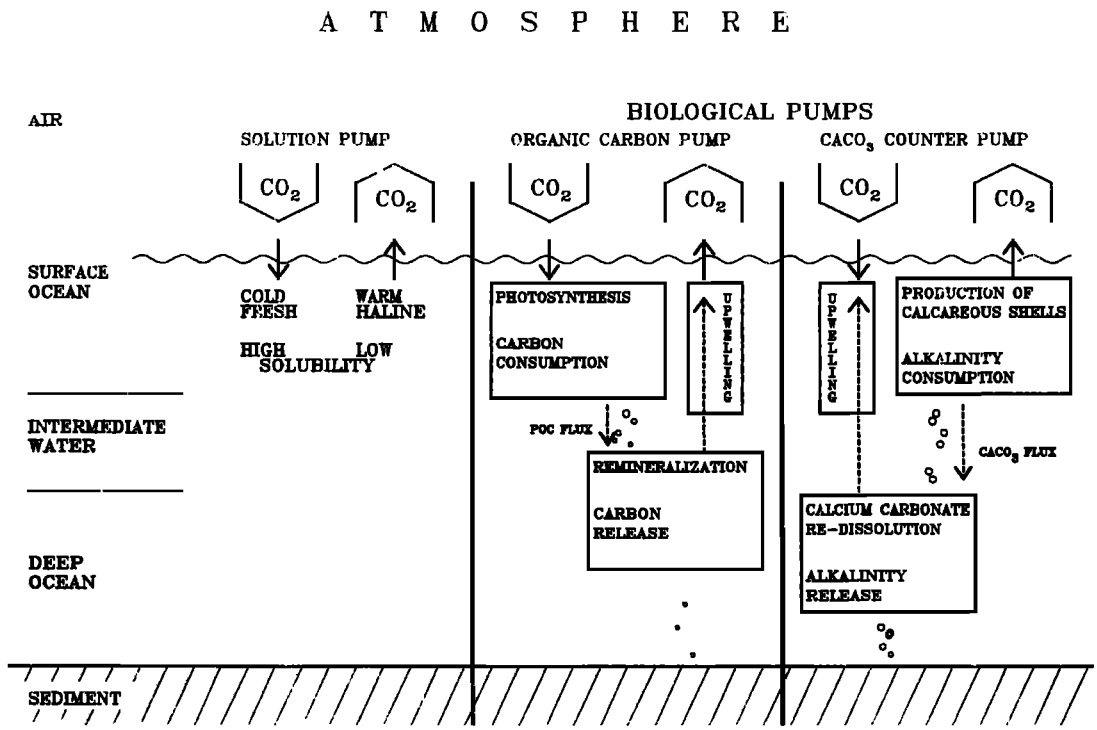

Fig. 1. Schematic diagram of the marine carbon pumps: the solution pump, the particulate organic carbon pump, and the $CaCO_3$ counter pump.

and the dynamical chemical equilibrium in the surface waters is shifted in the direction of higher CO_2 partial pressure [e.g., Baes, 1982].

The remnants of planktonic organisms (organic soft tissue or POC, $CaCO_3$ hard parts) sink through the water column, transferring carbon from the upper waters to the deep ocean. Due to remineralization of the organic carbon compounds, CO_2 and nutrients reenter the water column, and seawater pCO_2 rises. The upper layers of the world ocean are oversaturated with respect to $CaCO_3$. Dissolution of $CaCO_3$ hard parts occurs only in deeper layers (increasing pressure, decreasing temperature). $CaCO_3$ dissolution counteracts the effect of soft tissue remineralization and reduces seawater pCO_2. However, the $CaCO_3$ flux is only about a quarter of that of organic carbon on a mole to mole basis [Li et al., 1969]. An increase of alkalinity due to $CaCO_3$ dissolution in deep water may act as a process for the additional binding of atmospheric CO_2 with a strongly delayed response [Boyle, 1988].

Both $CaCO_3$ shells and organic carbon compounds partly enter the sediment layer at highly varying rates and ratios depending on their history in the upper water column.

Interconnected with these marine carbon cycle mechanisms is the redistribution of carbon components, nutrients, oxygen, temperature, and salinity within the wind-driven and thermohaline ocean circulation. The equatorial upwelling regions, for example, are net sources of atmospheric CO_2 due to the warming and degassing of cold deeper water [Oudot et al., 1987], while the Arctic and sub-Arctic deep-water production areas represent sinks for atmospheric CO_2.

In accordance with these mechanisms the hypotheses for causes of the glacial pCO_2 reduction in the atmosphere can be subdivided into four different groups concerned with: the solubility effect; the nutrient cycle; the $CaCO_3$ cycle; and the transport of chemical compounds by the oceanic velocity field.

An enhanced solubility for gaseous CO_2 in seawater during glacial times can be expected to explain at best a part of the CO_2 reduction. Broecker and Peng [1987b] discuss the possibility of a freshening of the surface ocean due to an in-

crease of sea ice production and a corresponding transfer of high-salinity water to the deep ocean ("salt pump"). Additionally, the mean glacial surface water temperature was about 1.7 K below the Holocene level [CLIMAP Project Members, 1981]. Both effects would lead to an increase of CO_2 solubility in seawater. On the other hand, the mean salinity during glacial times is estimated to have been about 4% higher than the interglacial level, due to enhanced storage of fresh water in the big ice sheets. A 4% salinity increase in surface waters would almost cancel the solubility increase due to the 1.7 K cooling of the sea surface temperature [Broecker and Peng, 1986]. In summary, the solubility effects are not expected to account for more than a few tens of parts per million of the atmospheric pCO_2 reduction.

Three different nutrient scenarios have been suggested. Two of these try to explain the CO_2 reduction by an increased nutrient inventory in the glacial ocean and a correspondingly stronger action of the biological POC pump. Broecker [1982] proposed an additional transfer of the biolimiting nutrient phosphate into the ocean from shelf areas laid dry during glacial times and exposed to continental runoff. Correspondingly the biological organic carbon pump would have acted more strongly and would have transferred larger amounts of organic carbon to deeper layers. Broecker [1984] himself, however, later questioned this hypothesis in view of the short time scale of the order of 1000 years of the observed CO_2 changes in the atmosphere.

The effect of this mechanism could have been dampened considerably by the additional transfer of carbon (and not only nutrients) into the glacial ocean as pointed out by Berger and Keir [1984]. These authors presented instead the alternative denitrification hypothesis suggesting that a strong reduction of the nutrient nitrate in seawater and an associated weakening of the biological organic carbon pump could have occurred at the end of the ice age. According to this scenario, nitrogen could have been expelled to the atmosphere from shallow anoxic shelf regimes to the atmosphere through denitrification.

The third nutrient hypothesis suggests a possible change of the ratio of nutrient elements to organic carbon, the Redfield ratio P:N:C, in particulate biogenic organic matter (P. Weyl as cited by Broecker [1982]). In today's ocean, values of about 1:16:130 are observed for POC as well as for the dissolved substances in ocean water itself [Takahashi et al., 1985; Peng and Broecker, 1987; Minster and Boulahdid, 1987]. However, if, as suggested by Weyl and Broecker, more carbon atoms could be fixed to particulate matter for a given number of nutrient atoms, then more carbon could clearly be extracted from the surface layer than at present.

Two $CaCO_3$ hypotheses have been proposed; they suggest a change in the oceanic $CaCO_3$ inventory (coral reef hypothesis) or in the composition of biogenic particulate matter (rain ratio hypothesis). According to the coral reef hypothesis [Berger and Keir, 1984] the abrupt atmospheric CO_2 increase at the end of the glaciation was caused by strong $CaCO_3$ precipitation in the newly formed shelf regimes after reflooding of the shelf areas that lay above sea level during the ice age. Alternatively, a decreasing relative production of $CaCO_3$ hard parts in the surface ocean could also have lowered the atmospheric CO_2 content during the glaciation (reduced rain ratio C_{CaCO3}:$C_{organic}$ [Berger and Keir, 1984; Dymond and Lyle, 1985]). As an additional process coupled to a possible increase of the biological pump, dissolution of $CaCO_3$ in response to enhanced organic oxidation in deep waters would increase oceanic alkalinity and would therefore also contribute to a lowering of the atmospheric CO_2 content during the glacial [Boyle, 1988].

The hypotheses concerned with a change in the oceanic velocity field may be introduced by beginning with the polar nutrient scenarios. While the surface waters of today's ocean show low concentrations of dissolved nutrients at low latitudes, high-latitude surface layers have a nutrient potential that is only partially used by biota. This may be due to the combined effect of convective overturning and more severe living conditions for marine organisms at high latitudes [Knox and McElroy, 1984]. If these nutrients could also be used for production of particulate organic carbon, then the ocean surface pCO_2 would be lowered. As possible mechanisms for a greater polar nutrient depletion an enhanced horizontal exchange of polar and subpolar waters with waters of temperate zones or a decrease of deep-water production have been suggested [Knox and McElroy, 1984; Sarmiento and Toggweiler, 1984; Siegenthaler and Wenk, 1984]. Broecker and Peng [1989] favor instead an increase of surface water alkalinity in the Southern Ocean as the more probable polar scenario.

Besides the polar scenarios a general weakening of the deep-ocean circulation would also lead to a pCO_2 reduction due to a more effective accumulation of biogenic particulate matter in deep layers [Broecker and Peng, 1987a]. Measurements of ^{14}C in planktonic and benthic foraminifera buried in the sediment provide evidence that a reduction of deep-sea ventilation indeed took place [Shackleton et al., 1988; Broecker et al., 1988; Broecker et al., 1990]. These data, together with reconstructions of the $\delta^{13}C$ distribution in the ice age ocean and Cd/Ca analyses, furthermore suggest a shift in the advective pattern and a more pronounced vertical fractionation between well-ventilated upper and intermediate waters and a less well ventilated bottom water regime [Duplessy et al., 1988; Boyle, 1988; Boyle and Keigwin, 1987] combined with a reduction [Curry and Lohmann, 1982] or even destruction [Shackleton et al., 1983] of the contrast between deep Pacific and deep Atlantic water masses.

Sarnthein et al. [1988] discuss an intensification of low latitude upwelling induced by a strengthening of the trade winds with a correspondingly enhanced nutrient supply to the surface ocean as an additional sink for atmospheric CO_2 during the last glaciation.

The observational evidence for a change of the ocean carbon cycle during the past is derived from ^{13}C and $CaCO_3$ saturation analyses of sediment core samples.

The marine $\delta^{13}C$ distribution is governed by fractionation effects and is generally inversely proportional to the nutrient distribution. Both the $\delta^{13}C$ and the PO_4 distributions depend on the efficiency of the biological POC pump, the pattern of remineralization in the water column, and the velocity field (increasing nutrient concentration and decreasing $\delta^{13}C$ values with increasing age of a water mass). For ^{13}C we consider two separate variables: vertical differences in $\delta^{13}C$ ($\Delta\delta^{13}C_{\mathrm{planktonic-benthic}}$ or briefly $\Delta\delta^{13}C_{p-b}$) and horizontal differences in benthic $\delta^{13}C$ between separate deep water masses ($\Delta\delta^{13}C_{\mathrm{benthic(1)-benthic(2)}}$ or briefly $\Delta\delta^{13}C_{b(1)-b(2)}$). The $\Delta\delta^{13}C_{p-b}$ values depend on the individual surface and deep-water species as well as on the specific surface and deep water growth conditions that vary regionally. Therefore $\Delta\delta^{13}C_{p-b}$ data are more difficult to interpret than $\Delta\delta^{13}C_{b(1)-b(2)}$ data.

The deep-sea $CaCO_3$ record reflects several processes: the production rate of $CaCO_3$ in the surface ocean, the rain ratio C_{CaCO3}:$C_{organic}$ (number of C atoms bound to $CaCO_3$ hard parts divided by C atoms bound to organic matter) in planktonic biota, and the degree of $CaCO_3$ saturation in the water column, which itself is a function of the remineralization rate of particulate organic carbon. Different $CaCO_3$ saturation indices are used, either the percentage of weight of $CaCO_3$ in the sediment or species dependent dissolution indices.

All scenarios for the pCO_2 reduction are subject to considerable drawbacks and uncertainties (see Broecker and Peng [1986] for a comprehensive discussion). They either call for an improbably strong change in one of the carbon cycle parameters or are not directly supported by observations and are based on untested assumptions. The modeling exercise in this paper is an attempt to provide a more quantitative assessment of the various hypotheses on glacial pCO_2 reduction in the light of available data.

2. MODEL STUDIES

2.1. *Model Description*

The model used in this study is the annually averaged version of the Hamburg Carbon Cycle Model. This model is based on the three-dimensional velocity and thermohaline fields of the Hamburg Large-Scale Geostrophic OGCM and uses the same grid. Both models are described in detail elsewhere [Maier-Reimer and Hasselmann, 1987; Maier-Reimer et al., unpublished data, 1991; Maier-Reimer and Bacastow, 1990; Bacastow and Maier-Reimer; 1990]. Therefore only a brief outline of the models' design is presented.

The models use a 72 x 72 grid (approximate 3.5° x 3.5° horizontal resolution) and 11 layers (intercepts at 0, 50, 112.5, 200, 350, 575, 850, 1500, 2500, 3500, 4500, and 6000 m). The OGCM velocity, temperature and salinity fields for the carbon cycle model were taken from a circulation model run (Maier-Reimer et al., unpublished data, 1991) with wind forcing using Hellermann and Rosenstein [1983] monthly mean winds, surface salinity forcing with data from Levitus [1982] and a surface temperature forcing using air temperatures from the comprehensive ocean-atmosphere data set (COADS) [Woodruff et al., 1987]. The circulation model

was integrated up to quasi steady state conditions (15,000 years, time step = 1 month).

The circulation model uses the primitive equations with an implicit integration scheme which retains baroclinic Rossby waves, as the climatically most relevant type of oceanic motion, and strongly damps fast propagating waves. A thermodynamical ice model is included, providing brine release and a corresponding upper water density increase during freezing. Diffusion occurs mainly through numerical diffusion caused by the advection scheme. This yields a diffusion which increases proportionally to the current velocities (which is also observed in nature). Static instability is treated by convective adjustment: If the density in a lower layer is smaller than in the layer above it at any grid point, salt and heat are exchanged between the two grid cells under conservation of salt and heat.

As the carbon cycle model uses a 1 year time step, annual mean values of velocity, temperature, and salinity fields and annual sums of convective overturning intervals (integrated convective adjustment parameters for each grid cell) were taken as input for the carbon cycle model. The velocity field for the control run differs from the original field presented by Maier-Reimer and Hasselmann [1987]; the updated circulation given by Maier-Reimer et al. (unpublished data, 1991) yields a more pronounced production of North Atlantic Deep Water and hence a more realistic flow pattern.

The carbon cycle model is illustrated in Figure 2. Three carbon reservoirs consisting of the atmosphere, ocean, and sediment are considered. The atmosphere is treated as a zonally averaged single layer governed by a meridional diffusive CO_2 transport and the ocean-atmosphere CO_2 exchange. The ocean-plus-sediment model consists of the inorganic part of the marine carbon cycle as described by Maier-Reimer and Hasselmann [1987] and a simple trophic model (largely following Broecker and Peng [1982]; see also Bacastow and Maier-Reimer [1990]) including $CaCO_3$ chemistry and interaction with sediment pools [Maier-Reimer and Bacastow, 1990].

The model tracer variables include atmospheric pCO_2, $\sum CO_2$ (total dissolved inorganic carbon), total alkalinity, PO_4 (as biolimiting nutrient), POC (particulate organic carbon, plankton soft tissue), and particulate $CaCO_3$ (plankton calcareous hard parts). For all carbon species, three carbon isotopes (the stable ^{12}C and ^{13}C and radiocarbon ^{14}C) are considered.

The basic processes considered by the carbon cycle model are: gas exchange between ocean and atmosphere, advection (and mixing) by the oceanic velocity field, diffusive carbon transport in the atmosphere layer, new production of POC (defined as the amount of newly formed biomass which is transferred from the surface layer into deeper layers each year and is thereby removed from the seasonal ocean-atmosphere exchange cycle), calcite production, remineralization of POC, dissolution of $CaCO_3$, particle flux through the water column, sedimentation, and resuspension from the sediment by bioturbation. Details, indicating also modifications relative to previous descriptions, are given in the appendix.

2.2. *Control Run*

As reference base for the sensitivity experiments a control or reference run was carried out. The model parameters and tracer inventories for the reference run have been chosen in order to reproduce principal features of the preindustrial ocean (i.e., to represent the ocean without anthropogenic disturbances like bomb radiocarbon and fossil fuel or land use carbon). The inventories of different tracers were adjusted so that the preindustrial value for atmospheric pCO_2 was achieved. The choice of the other parameters is given in the appendix. The model value for atmospheric pCO_2 became stationary at 278.5 ppm. As the development of some model parameterizations is not considered as finished, we do not judge this reference run as optimal. Nevertheless, it reproduces the basic tracer patterns in the ocean rather well.

As examples from the control run, Figures 3–6 show $\delta^{13}C$ of total dissolved inorganic CO_2 and CO_3^{2-} concentration along sections close to positions of the GEOSECS Western Atlantic and Western Pacific meridional sections [Bainbridge, 1981; Broecker et al., 1982; Kroopnick, 1985]. The calcite lysocline calculated from the model $[CO_3^{2-}]$ value and the critical CO_3^{2-} concentration given by Broecker and Takahashi [1978] is also shown in the CO_3^{2-} plots. The principal patterns of the present ocean are reproduced in the model sections. The relatively young North Atlantic Deep Water (NADW), which originates in the sub-Arctic and Arctic regions of the North

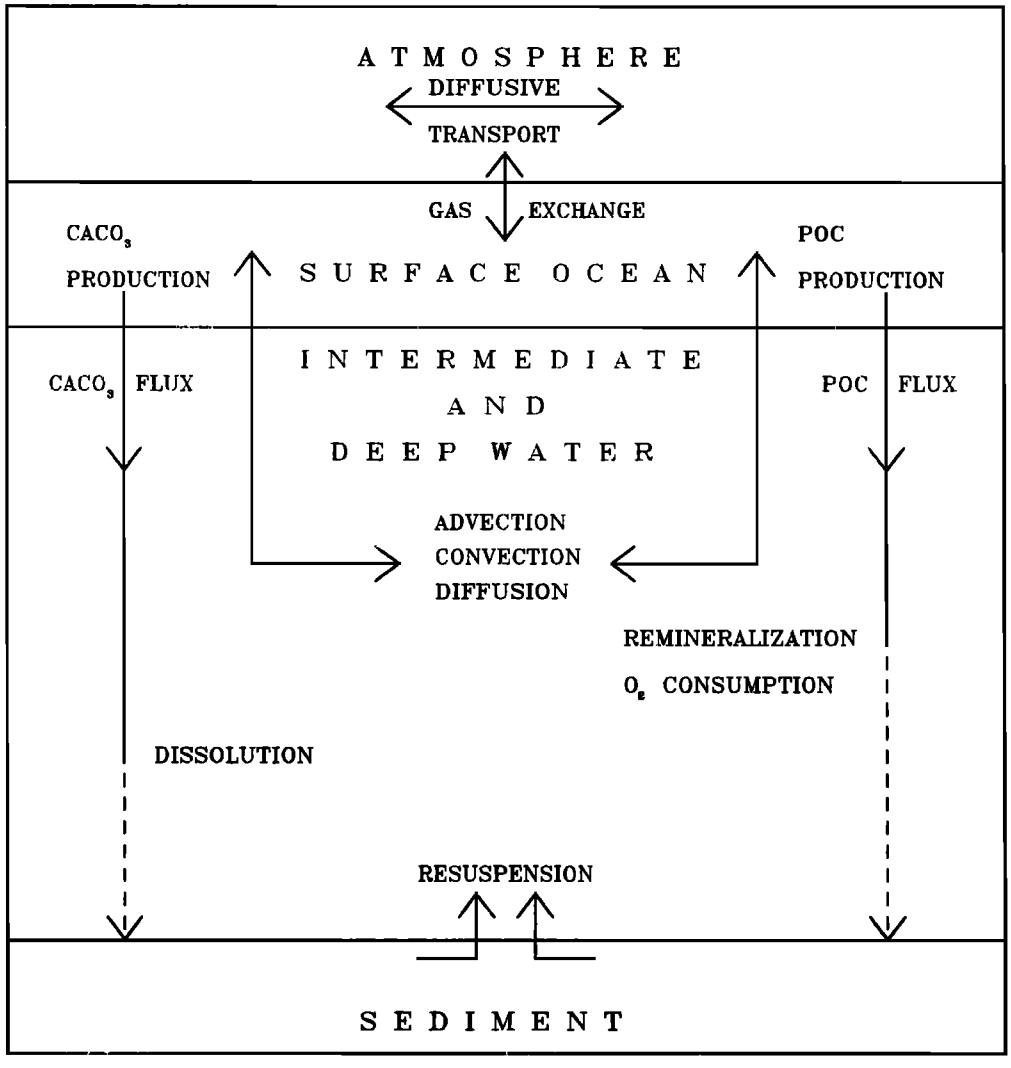

Fig. 2. Schematic diagram of the model concept showing the reservoirs and processes that are considered.

Atlantic, shows relatively high $\delta^{13}C$ values because it has not yet been exposed to large fluxes of remineralized organic carbon (Figure 3). NADW correspondingly shows high CO_3^{2-} concentrations, i.e., a tendency toward high $CaCO_3$ preservation (Figure 5). Antarctic Bottom Water in the abyssal South Atlantic shows increased corrosivity for $CaCO_3$ and lower $\delta^{13}C$ values, as its primary source is not young surface water [Weiss et al., 1979]. Proceeding from the south to the deep waters of the northern Pacific, the $\delta^{13}C$ level sinks more and more, indicating a growing level of organic matter remineralization (Figure 4). As acidity of seawater increases in association with this process, more deep-water CO_3^{2-} ions, together with the free carbon dioxide, are transformed into bicarbonate, resulting in a shallower $CaCO_3$ saturation level in the deep Pacific compared to deep Atlantic waters (Figure 6).

2.3. *Sensitivity Experiments*

The model's sensitivity to changes Δx_j in the parameters x_j which were regarded as the most critical for regulating the atmospheric pCO_2 was determined by a set of nine sensitivity experiments. Each of the sensitivity runs was integrated for 20,000 years to a stationary state. The computing time was 20 CRAY-2S cpu hours per run. The long integration time was necessary to

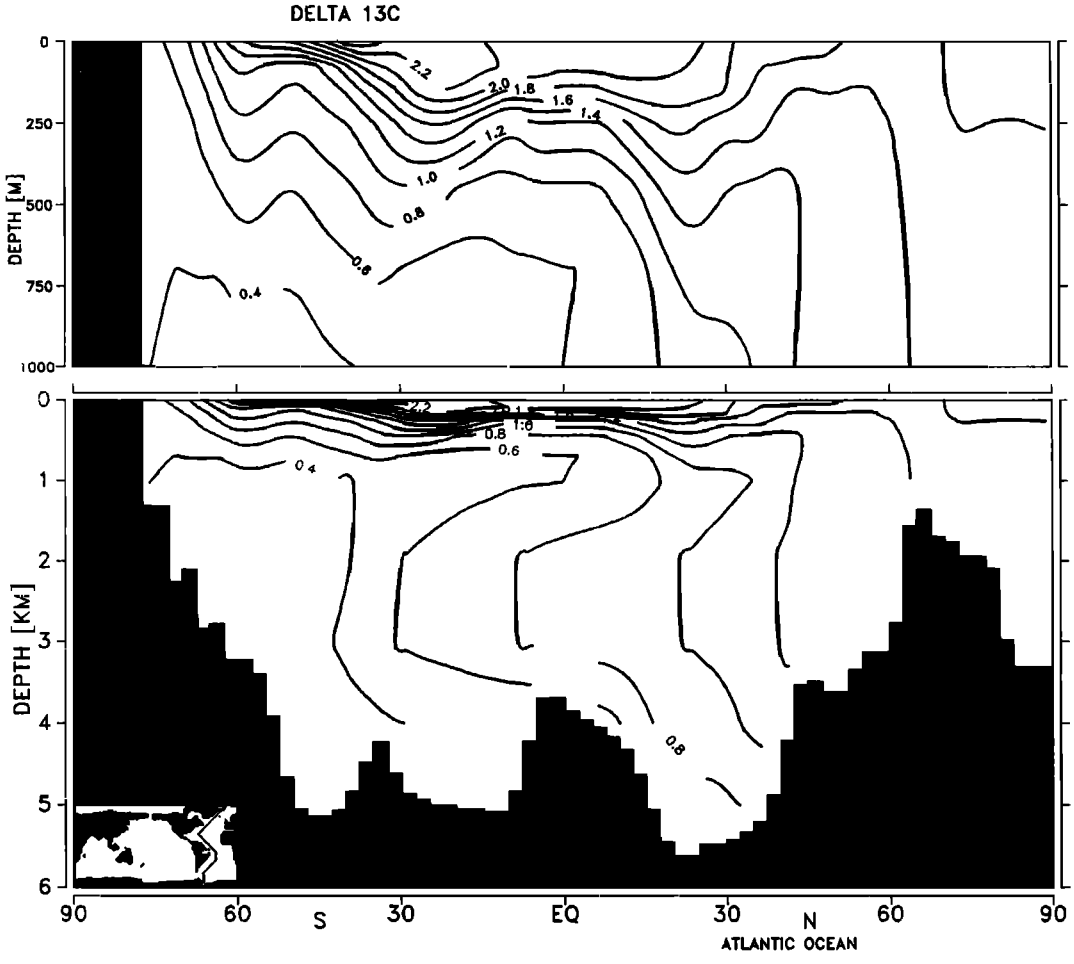

Fig. 3. $\delta^{13}C$ of $\sum CO_2$ (in per mil) of the model reference run in a cross section close to the position of the Western Atlantic GEOSECS section.

equilibrate the $CaCO_3$ sediment pool. In each experiment one parameter (parameter changes Δx_j, $j = 1, \ldots, 9$) was changed as follows:

j = 1 Increase of biological productivity at high latitudes:
$\Delta x_1 = 2.0$;
$I_l(\phi \geq 50°) =$
$I_l(\phi)^{\text{control}} + \Delta x_1 \cdot (I_l(\phi)^{\text{control}}_{\text{max}} - I_l(\phi)^{\text{control}})$
(I_l is a parameter characterizing plankton growth growth conditions, see appendix.)

j = 2 30% reduction of the Redfield ratio P:C:
$\Delta x_2 = 36.6$; $x_2 = \frac{P}{C} = \frac{1}{122+\Delta x_2}$

j = 3 30% increase of the PO_4 inventory (30% increase of the initial PO_4 concentration):
$\Delta x_3 = 0.3$; $x_3 = [PO_4]_{\text{control}} + [PO_4]_{\text{control}} \cdot \Delta x_3$

j = 4 Additional input of 1231 GtC POC (this corresponds to the same number of P atoms as added in the PO_4 inventory experiment):
$\Delta x_4 = 1231$ GtC; $x_4 = \int [POC]_{\text{control}}\, dV + \Delta x_4$

j = 5 Additional input of 2462 GtC $CaCO_3$ (this corresponds to twice the amount of additional C input into the ocean as in the POC inventory experiment):
$\Delta x_5 = 2462$ GtC; $x_5 = \int [CaCO_3]_{\text{control}}\, dV + \Delta x_5$

j = 6 50% decrease of the rain ratio C_{CaCO3}:C_{organic}:
$\Delta x_6 = -0.125$; $x_6 = \left(\frac{C_{CaCO3}}{C_{\text{organic}}}\right)_{\text{control}} + \Delta x_6$

j = 7 2 K reduction of sea surface temperature (this implies a change of all temperature dependent chemical constants, including the solubility coefficients for gaseous CO_2):
$\Delta x_7 = -2.0$ K; $x_7 = SST_{\text{control}} + \Delta x_7$

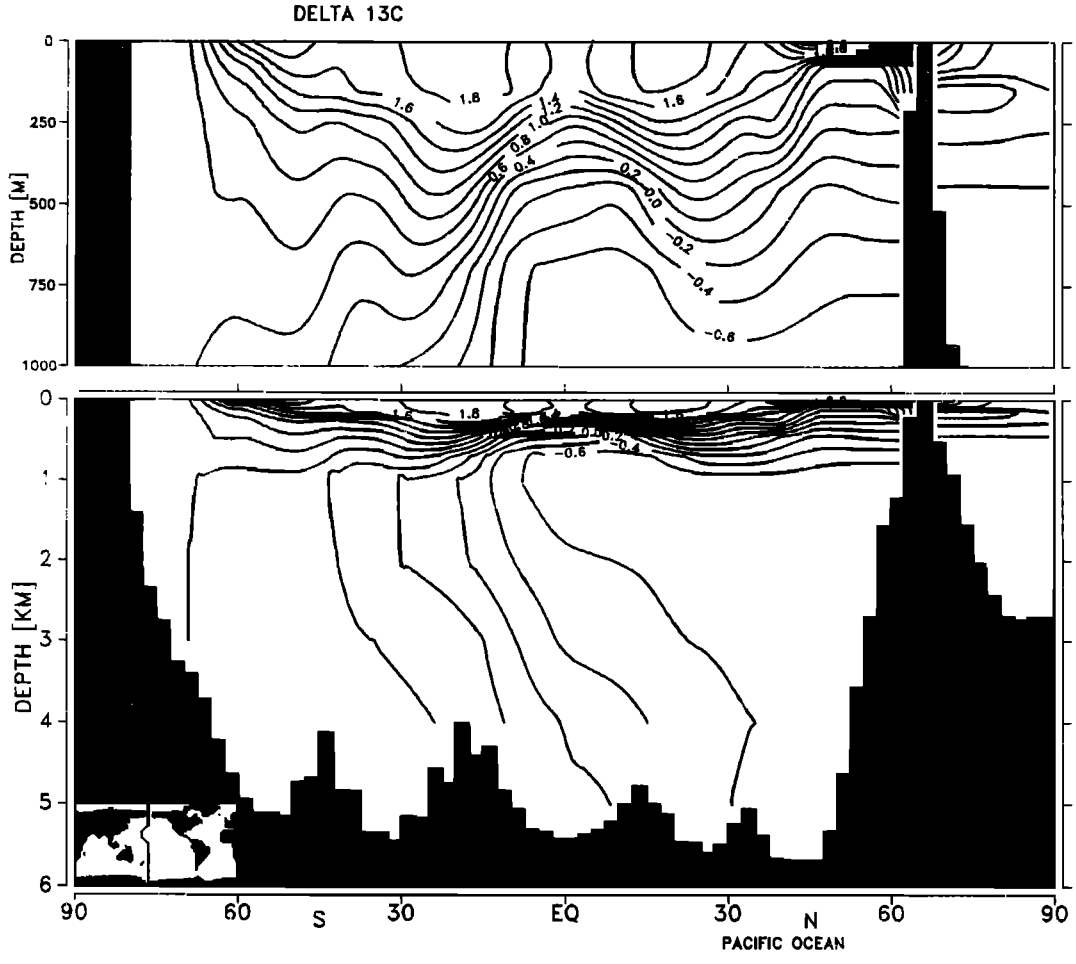

Fig. 4. $\delta^{13}C$ of $\sum CO_2$ (in per mil) of the model reference run in a cross section close to the position of the Western Pacific GEOSECS section.

j = 8 50% reduction of ocean ventilation (50% reduction of current velocities):
$\Delta x_8 = -1.0$; $x_8 = \vec{v}_{control} \cdot 2^{\Delta x_8}$

j = 9 Change of the advective circulation pattern to an alternate "paleoocean" regime:
$\Delta x_9 = 1.0$;
$x_9 = \vec{v}_{control} + \Delta x_9 \cdot (\vec{v}_{"paleo"} - \vec{v}_{control})$

The first experiment simulates polar nutrient depletion. Experiments 2–4 address changes in the nutrient cycle corresponding to the Redfield ratio scenario (experiment 2), the PO_4 inventory (or inverse denitrification) scenario (experiment 3), and the POC inventory scenario (PO_4 plus $\sum CO_2$ increase, experiment 4). Experiments 5 and 6 are $CaCO_3$ experiments representing, respectively, the (inverse) coral reef and the rain ratio scenario. Scenario 7 is a test of a (temperature induced) change of the solution pump.

Finally, to investigate the influence of the ocean circulation on the atmospheric pCO_2, two carbon cycle model runs were carried out with the same carbon chemistry as in the control run but with different velocity fields (experiments 8 and 9). First, a general decrease of the current velocities by 50% was investigated. Second, the circulation field for another stable mode of ocean operation was taken as input. This circulation was achieved using the same surface forcing as in the control run but with a different choice of salinity initial conditions. Before starting that model run, 1 per mil of salinity was subtracted at all ocean grid points north of 30°N. Exactly the same amount of salt was added to the grid points south of 30°S, so that the total salinity in-

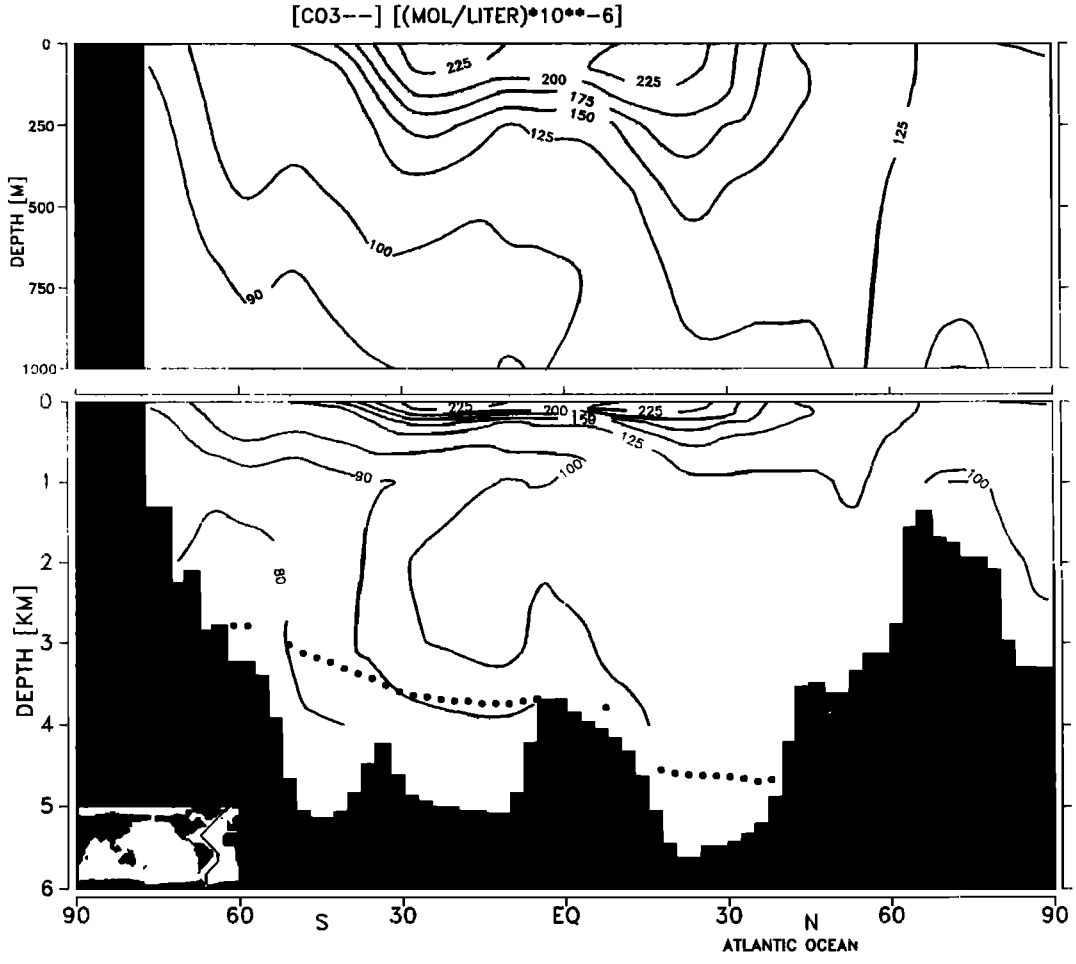

Fig. 5. CO_3^{2-} concentration (in micromoles per liter) of the model reference run in a cross section close to the position of the Western Atlantic GEOSECS section. The modeled calcite lysocline is indicated by the dotted line. (Contour intervals are 10 for concentrations less than 100 μmol/L and 25 otherwise.)

ventory of the control run was conserved (Mikolajewicz, personal communication, 1990). The surface forcing was retained as for the control run. The existence of different stable modes of ocean circulation for the same surface forcing but different initial conditions has been predicted theoretically by Stommel [1961], Rooth [1982] and Marotzke et al. [1988] and has been found in earlier model experiments by Bryan [1986].

While the field of motion with a 50% reduction in current velocities has an identical pattern to the control run but a more sluggish circulation (and hence a decreased ventilation), the second stable mode velocity field is marked by a basically different advective pattern, with significant reduction of North Atlantic Deep Water production. This is illustrated by the control run values and the anomaly fields for the conventional radiocarbon ages shown in Figures 7–12. A reduction in deep-sea ventilation and a change in the advective pattern have been inferred from isotopic analyses of sediment core samples [e.g., Duplessy et al., 1975; Shackleton et al., 1983] and are substantiated by recent sedimentary investigations [e.g. Boyle and Keigwin, 1987; Curry et al., 1988; Duplessy et al., 1988; Shackleton et al., 1988; Broecker at al., 1988, 1990]. The $\delta^{13}C$ Atlantic Ocean cross sections for both circulation experiments are given in Figures 13 and 14 (all $\delta^{13}C$ values were calibrated so that $\delta^{13}C = -6.5$ per mil for the model atmosphere).

Tables 1 and 2 and Figure 15 summarize the

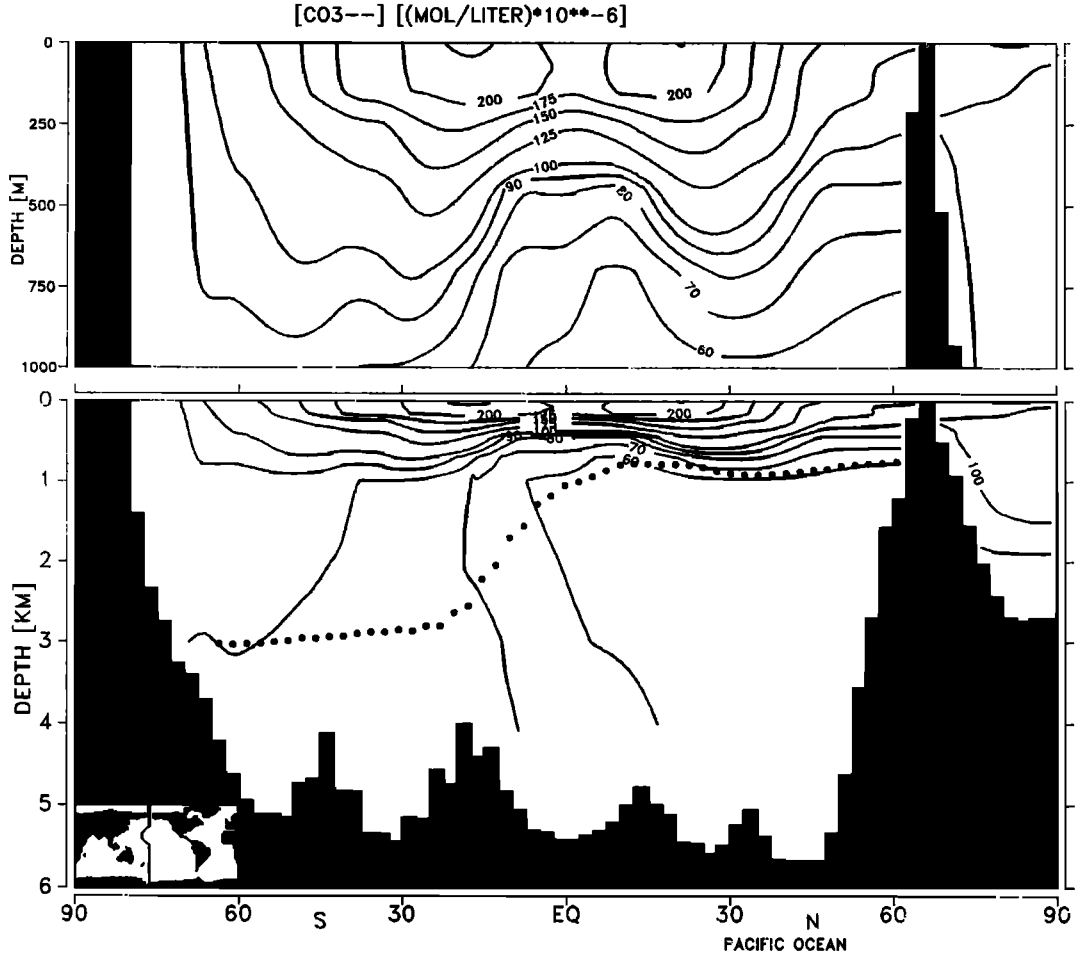

Fig. 6. CO_3^{2-} concentration (in micromoles per liter) of the model reference run in a cross section close to the position of the Western Pacific GEOSECS section. The modeled calcite lysocline is indicated by the dotted line. (Contour intervals are 10 for concentrations less than 100 μmol/L and 25 otherwise.)

sensitivity study results for atmospheric CO_2 partial pressure and new production.

The control run yields a global new production rate of 8.99 GtC/yr. This value is higher than the rate of 3.4–4.7 GtC/yr deduced by Eppley and Peterson [1979] from observations. However, Packard et al. [1988] compute a new production value of 21.9 GtC/yr from ETS measurements which is close to estimates of total primary production [see Romankevich, 1984; De Vooys, 1979]. On the basis of marine nitrogen studies, Longhurst and Harrison [1988] suggest a possible new production rate which is twice the value reported in Eppley and Peterson [1979]. The modeled absolute new production rate lies within this broad range of observational results, which are not yet able, however, to provide a critical test of the model.

For the nutrient cycle scenarios the reduction in pCO_2 is a direct consequence of an increase in biological production (Figure 15). The POC inventory experiment yields the same change in new production as the PO_4 inventory experiment but only a weak pCO_2 decrease. This experiment clearly shows that the impact on atmospheric pCO_2 predicted by the PO_4 inventory scenario [Broecker, 1982] breaks down if not only PO_4 but also organic carbon compounds are transferred from the shelf regions (which lie dry during glaciation) into the open ocean [cf. Berger and Keir, 1984]. By remineralization of these organic compounds, additional carbon is intro-

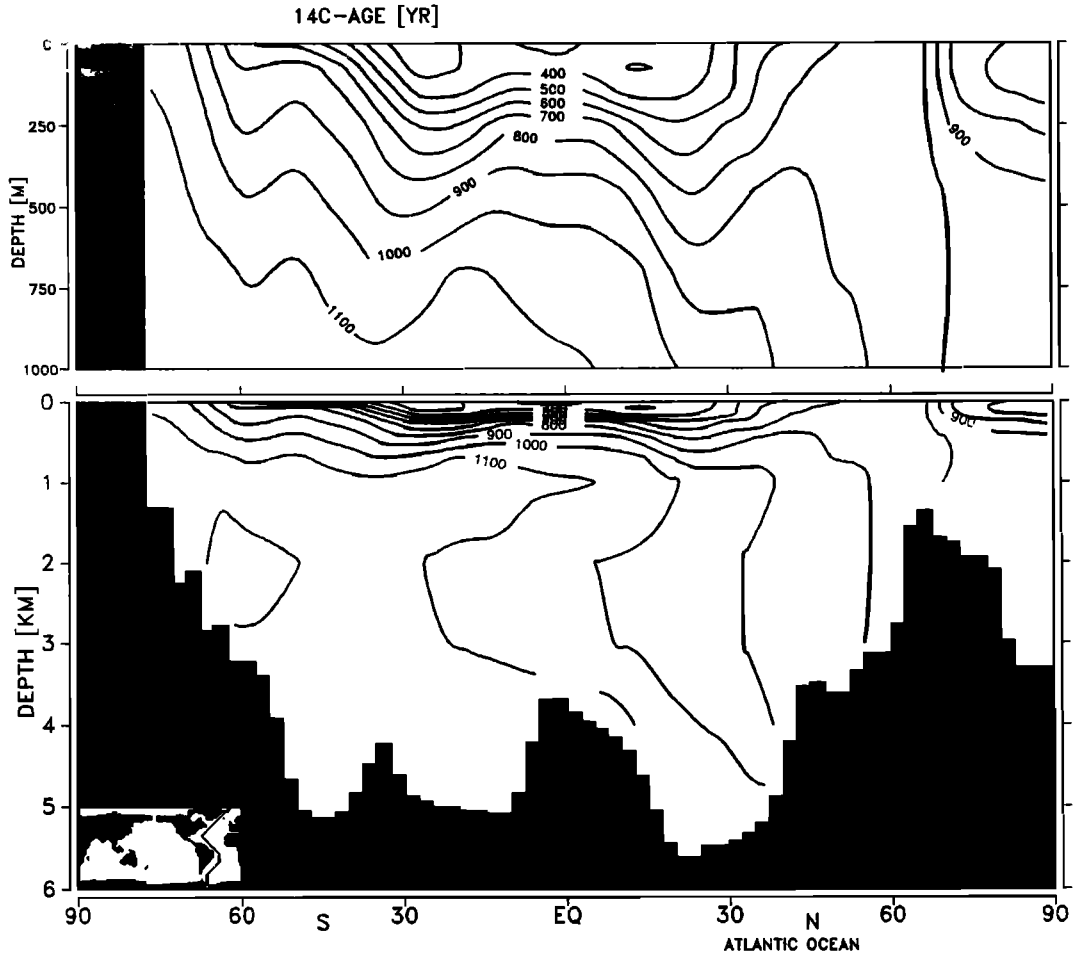

Fig. 7. Conventional radiocarbon ages (in years) for the control run. Atlantic Ocean.

duced into the inorganic oceanic carbon reservoir, thus counteracting the strengthening of the biological organic carbon pump due to the increase in nutrient availability.

The rain ratio, $CaCO_3$ inventory, and solubility (sea surface temperature reduction) scenarios show a reduction of atmospheric pCO_2 without changing new production.

The circulation scenario with a change in the advective pattern leads to a slight pCO_2 reduction and an only negligible change in global new production. The ventilation reduction experiment, in contrast, yields a lowering of the atmospheric CO_2 with a parallel decrease in new production. This result is interesting, as most glacial pCO_2 scenarios argue from an increased biological pump and an associated increase in new production. Two effects may lead here to the parallel decrease in atmospheric pCO_2 and new production. First, the slower global ocean circulation causes a higher accumulation of carbon and nutrients in deeper layers than in the control run. This causes a reduction of pCO_2 for a given level of new production. However, new production is actually also decreased (but not as much as the velocities) due to the slower supply of nutrient rich waters from the deep. Second, the increase of total CO_2 in the deep ocean leads to an increase of alkalinty due to the enhanced dissolution of suspended particulate $CaCO_3$ and $CaCO_3$ sediment. This alkalinity increase inhibits outgassing of CO_2 in upwelling areas, thereby also contributing to a pCO_2 reduction in the atmosphere.

3. COMPARISON OF MODEL RESULTS WITH PALEOCLIMATE DATA

The results of the sensitivity studies were compared with observational data from marine sed-

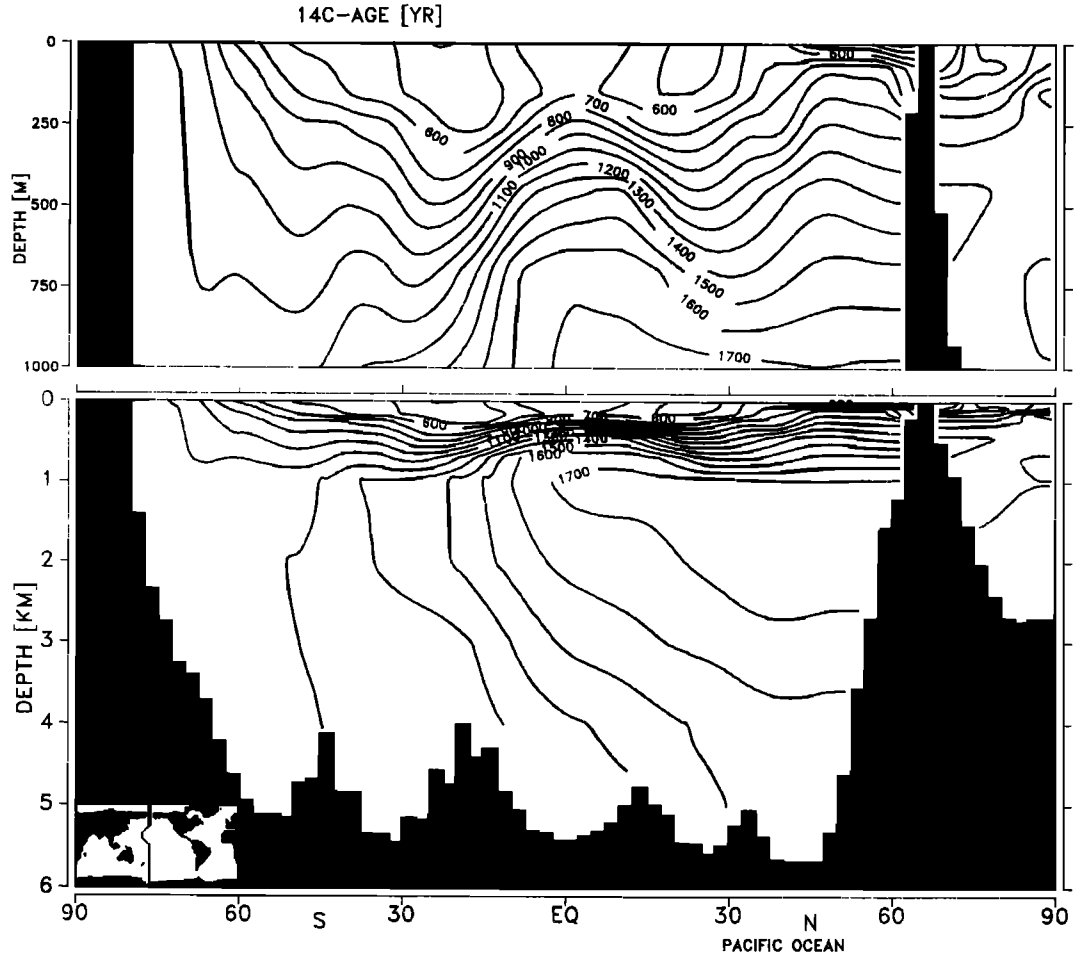

Fig. 8. Conventional radiocarbon ages (in years) for the control run. Pacific Ocean.

iment core and ice core analysis. We considered four types of paleo-climate records: (1) atmospheric pCO_2, (2) $\Delta\delta^{13}C_{p-b}$ ($\delta^{13}C$ difference between upper and deep waters), (3) $\Delta\delta^{13}C_{b(1)-b(2)}$ ($\delta^{13}C$ difference between different deep water masses), and (4) $CaCO_3$ saturation.

We compared the deviations of the modeled tracer distributions from their control run values with the deviations of observed tracer distributions from their preindustrial, or interglacial, values.

3.1. *Data Base*

The sources for compilation of the observed data base are listed in Table 3 and 4 for the ^{13}C records and in Table 5 for the $CaCO_3$ records.

For atmospheric pCO_2 the Vostok ice core (east Antarctica) data were used [Barnola et al., 1987]. As error bounds we adopted the maximum of the upper and lower error boundaries cited by Barnola et al. [1987] (Figures 16 and 17).

For ^{13}C a number of $\Delta\delta^{13}C_{p-b}$ and $\Delta\delta^{13}C_{b(1)-b(2)}$ curves from the Atlantic and Pacific Oceans were used (Table 4 and Figure 16). Both the $\Delta\delta^{13}C_{p-b}$ and the $\Delta\delta^{13}C_{b(1)-b(2)}$ curves were considered in the form of difference curves between two water masses and not as absolute values.

The observed planktonic $\delta^{13}C$ values were taken from analyses of calcareous tests of the foraminiferal species *Globigerinoides sacculifer* and, for the equatorial Pacific core V19-30, of *Neogloboquadrina dutertrei*. These species have different habitats. *Globigerinoides* dwells in the surface layer, while *Neogloboquadrina dutertrei* prefers a less nutrient depleted subsurface habitat and lives in a larger depth range, extending from the surface to below the thermocline [Fairbanks et al., 1982]. *Globigerinoides sacculifer* is

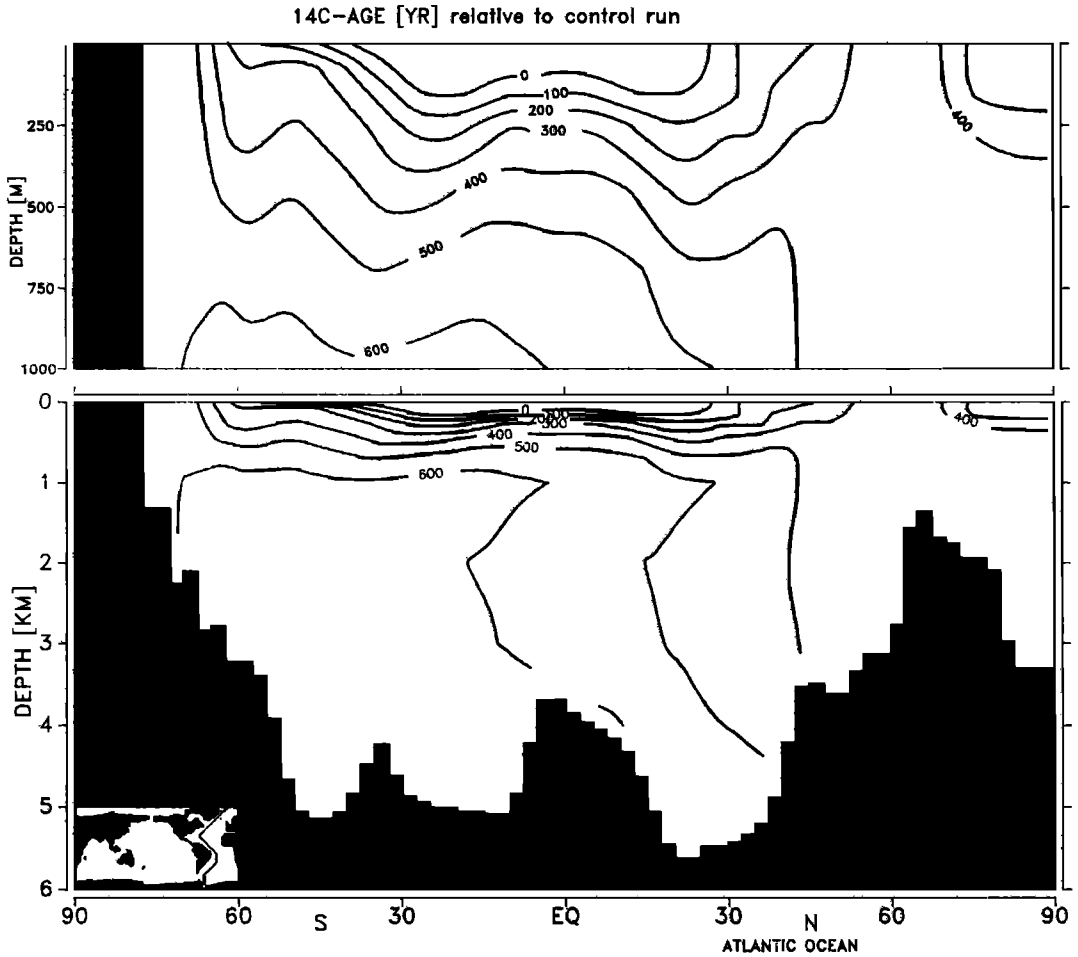

Fig. 9. Radiocarbon age difference (in years) between reduced ventilation experiment and control run. Atlantic Ocean.

therefore a more reliable indicator of surface water $\delta^{13}C$.

For benthic $\delta^{13}C$, analyses of the of the epifaunal *Cibicidoides* spp. shells reflect the $\delta^{13}C$ of the ambient bottom water in a more reliable way than data based on the infaunal *Uvigerina* spp. These organisms live within the uppermost sediment layer. The $\delta^{13}C$ content of their shell material may therefore be influenced by degradation of organic matter within the sediment and reflect the $\delta^{13}C$ value of the pore water rather than that of the overlying oceanic bottom water [e.g., Altenbach and Sarnthein, 1989]. The *Uvigerina*-based records [Shackleton et al., 1983; Shackleton and Pisias, 1985] are used here only for illustrating the quantitative differences to the corresponding *Cibicidoides* records.

The error of the $\delta^{13}C$ difference records was estimated from the analysis error. The total analysis error of one $\delta^{13}C$ difference pair is then given by $e = \sqrt{e_1 + e_2}$, where e_1 and e_2 are the analytical errors of the single planktonic or benthic values (Table 4). To allow for uncertainties in the chronology, the final error estimate was taken as twice e (Figure 16). For the stacked record of Atlantic $\Delta\delta^{13}C_{p-b}$ the standard deviation of 0.15 per mil was used as total error [Curry and Crowley, 1987].

The $\delta^{13}C$ records were synchronized with the corresponding $\delta^{18}O$ signals by application of the reference time scale of Martinson et al. [1987]. An exception is the benthic $\delta^{13}C$ record of core Sonne 12-98. As this core has a relatively poor time resolution, a chronology suggested by M. Sarnthein and K. Winn (personal communication, 1990) was adopted. The time scale adjustment using the Martinson et al. [1987] reference curve should result in a satisfactory relative syn-

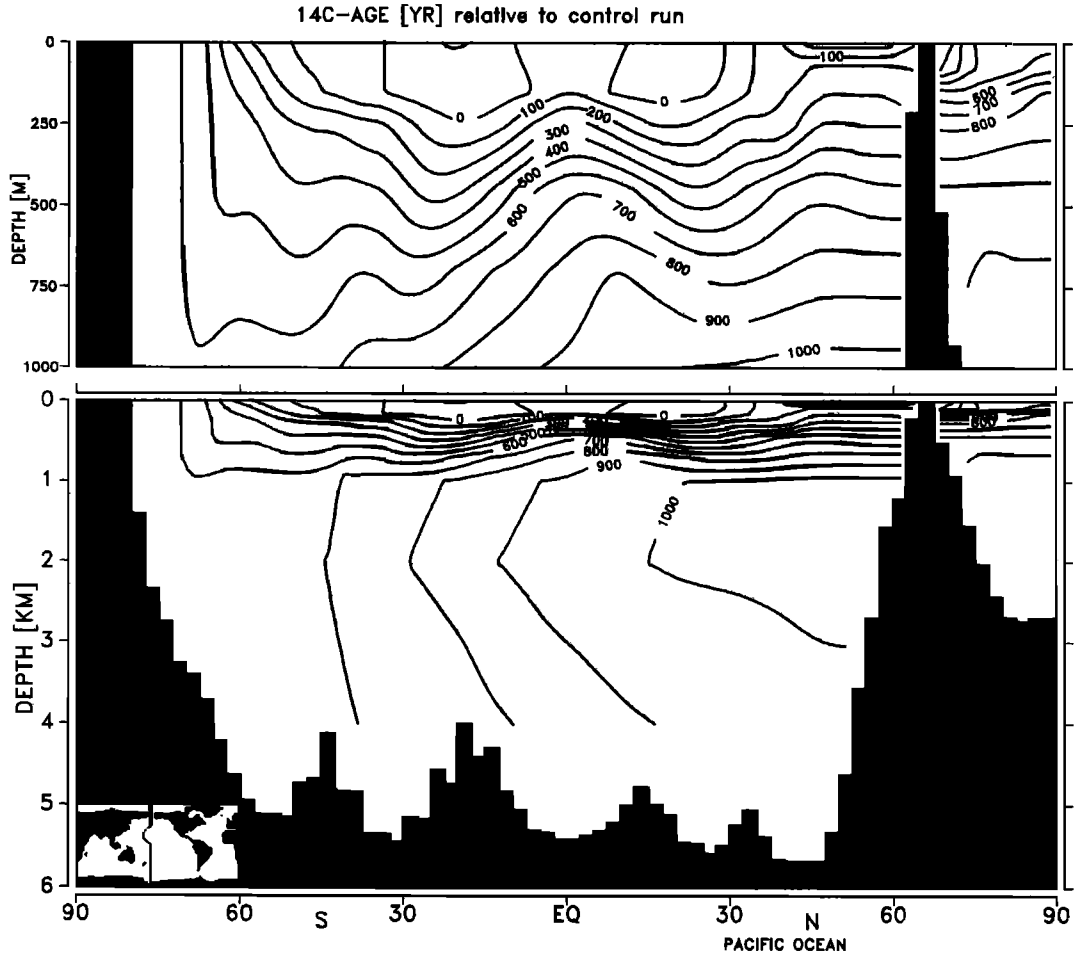

Fig. 10. Radiocarbon age difference (in years) between reduced ventilation experiment and control run. Pacific Ocean.

chronization of different time series but may not represent the optimum absolute time scale, especially for the postglacial period [cf. Bard et al., 1990].

In order to compare changes in $CaCO_3$ saturation between model and observations, we considered estimates for the variations of the calcite lysocline depth levels (Figure 17). The Indian Ocean lysocline curve [Peterson and Prell, 1985] is based on species-dependent dissolution indices (CDI, composite dissolution index). The Pacific Ocean lysocline time series was estimated from the average depth variations of the 40%-, 60%-, and 80%-$CaCO_3$ isolines as given by Farrell and Prell [1989]. The resulting average curve was adjusted to a mean lysocline depth lowering of 700 m during glacial conditions (18–65 kyr B.P.). For the northwestern Atlantic Ocean the lysocline depth curve suggested by Balsam [1983] was used. To estimate the northeastern Atlantic lysocline variations (Canary Basin), the variations in percentage of fragments of planktonic foraminifera and percentage of benthic foraminifera in the sediment reported by Crowley [1983] were taken as $CaCO_3$ dissolution indices. The curves were adjusted to allow for the estimated shallowing of the Canary Basin lysocline of about 300 m relative to Holocene values during oxygen isotopic stages 2 and 4 [Crowley, 1983].

The error boundaries for the lysocline change records (Figure 17) were estimated from the vertical core spacing for the Indian Ocean and the NW Atlantic. For the Pacific Ocean curve the error was assumed to be +/− 250 m. The error for the NE Atlantic record was estimated from the differences between the two dissolution index curves, but it was taken to be at least +/− 100 m.

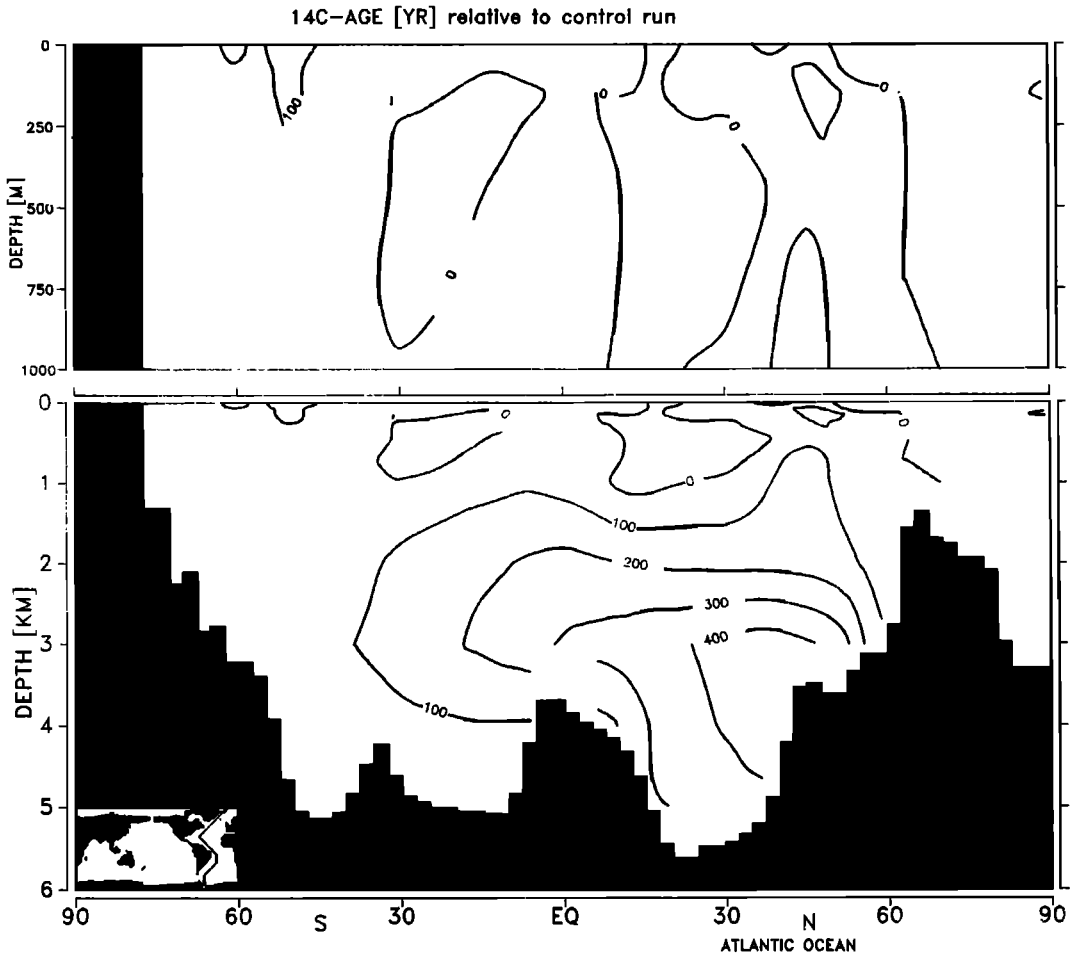

Fig. 11. Radiocarbon age difference (in years) between advective pattern change experiment and control run. Atlantic Ocean.

No chronology adjustment was carried out for the $CaCO_3$ and pCO_2 records. For the $CaCO_3$ records this should not lead to severe errors, since the lysocline depth variations show less variability on short time scales than do the ^{13}C time series. The Vostok ice core $\delta^{18}O$ chronology differs from the marine sediment core $\delta^{18}O$ chronologies [Lorius et al., 1985]; these differences are large only for the last interglacial period and the interglacial-glacial transition, while for the remainder of the last climatic cycle the correspondence between the marine and ice core chronologies is quite good. The chronology of the Vostok pCO_2 record [Barnola et al., 1987] is based on the Vostok $\delta^{18}O$ chronology and additional assumptions that may lead to further minor deviations from the marine time scales. At present there is no reliable method of deciding whether the differences between the time scales are due to different time evolutions of the different environments (and are therefore correct) or to errors in the dating method.

The $\Delta\delta^{13}C_{p-b}$ curves show strongest signals around 70 kyr B.P., where the pCO_2 curve also exhibits a pronounced decrease (Figure 16). Both Pacific $\Delta\delta^{13}C_{p-b}$ curves show elevated vertical $\delta^{13}C$ contrasts during glaciation. This is also true for the *Cibicidoides*-based Atlantic $\Delta\delta^{13}C_{p-b}$ record (core 13519 [Sarnthein et al., 1984; Zahn et al., 1986]) for most of the full glaciation period. The stacked record for equatorial Atlantic $\Delta\delta^{13}C_{p-b}$ [Curry and Crowley, 1987] is marked by a strong negative trend near 70 kyr B.P. and values around the interglacial level between 50 and 18 kyr B.P. For this record, however, the benthic $\delta^{13}C$ reference record of Pacific core V19-30 (and not an Atlantic benthic record) was used by Curry and Crowley [1987]. It should

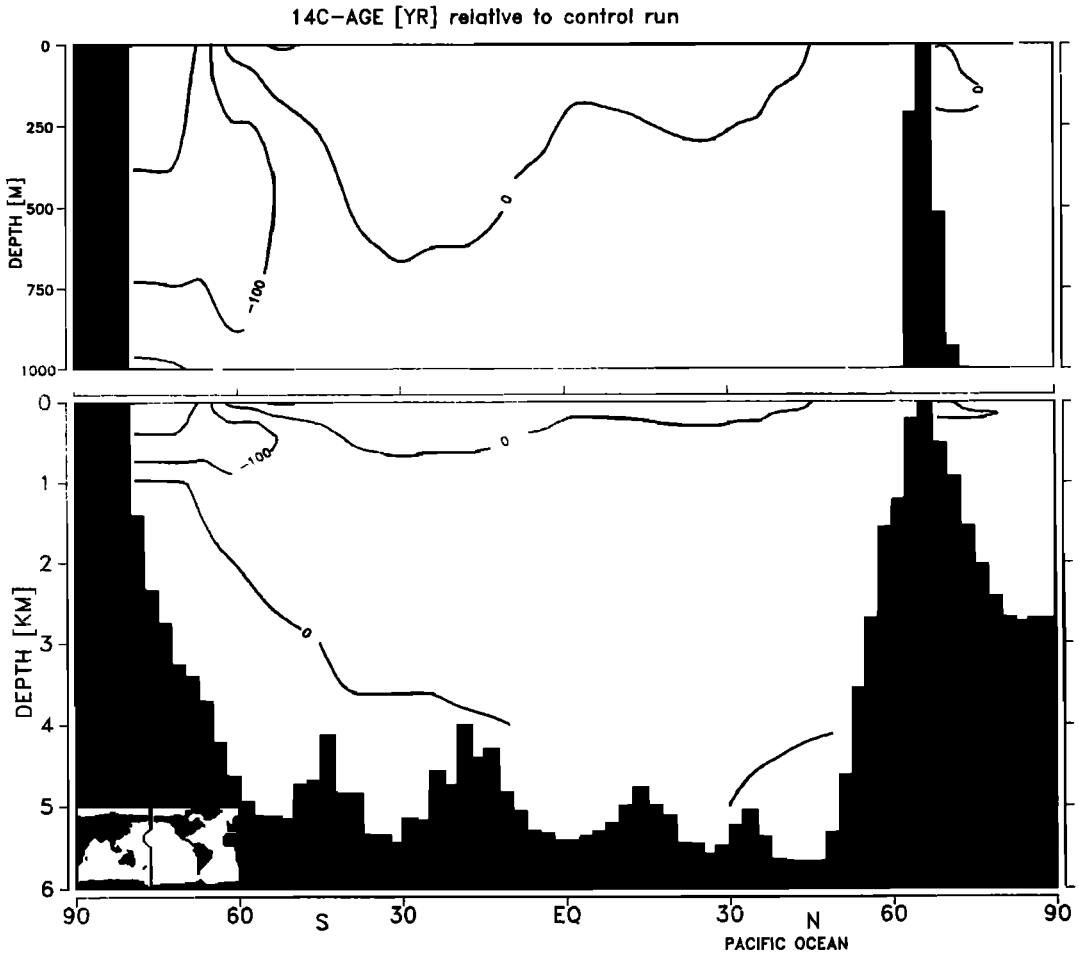

Fig. 12. Radiocarbon age difference (in years) between advective pattern change experiment and control run. Pacific Ocean.

be stressed again that the $\Delta\delta^{13}C_{p-b}$ signal is difficult to interpret because of the complex dependency on the individual growth conditions of the species used.

The two $\Delta\delta^{13}C_{b(Atl)-b(Pac)}$ curves indicate a reduced $\delta^{13}C$ contrast between the deep water masses of the Atlantic and Pacific oceans during full glaciation. The amplitude of the *Cibicidoides*-based record is only half that of the *Uvigerina*-based curve.

The calcite lysocline reconstructions also provide evidence for marked changes in the marine carbon cycle around 70 kyr B.P., where the most prominent atmospheric pCO_2 decrease occurred (Figure 17). The Indian Ocean record shows a strong dissolution spike during this period. The Indian Ocean and the Pacific Ocean records give evidence for an improved $CaCO_3$ preservation (high saturation) during glacial conditions. The two North Atlantic lysocline time series indicate an enhanced corrosion of $CaCO_3$ during glaciation, with two almost coherent oscillations. The amplitude of the NW Atlantic record, however, is almost 1 order of magnitude larger than that of the NE Atlantic curve.

Model tracer distribution changes were determined at the model grid points closest to the locations of the observed variations (except for atmospheric pCO_2, of course, where the global average model value was taken). $\Delta\delta^{13}C_{p-b}$ values were calculated by subtracting the respective model surface and bottom layer values. The Pacific planktonic $\delta^{13}C$ value was calculated from the local average of model layers 1 and 2, since the corresponding observed data were derived from the subsurface species *Neogloboquadrina dutertrei*.

Calcite lysocline depth levels were calculated as

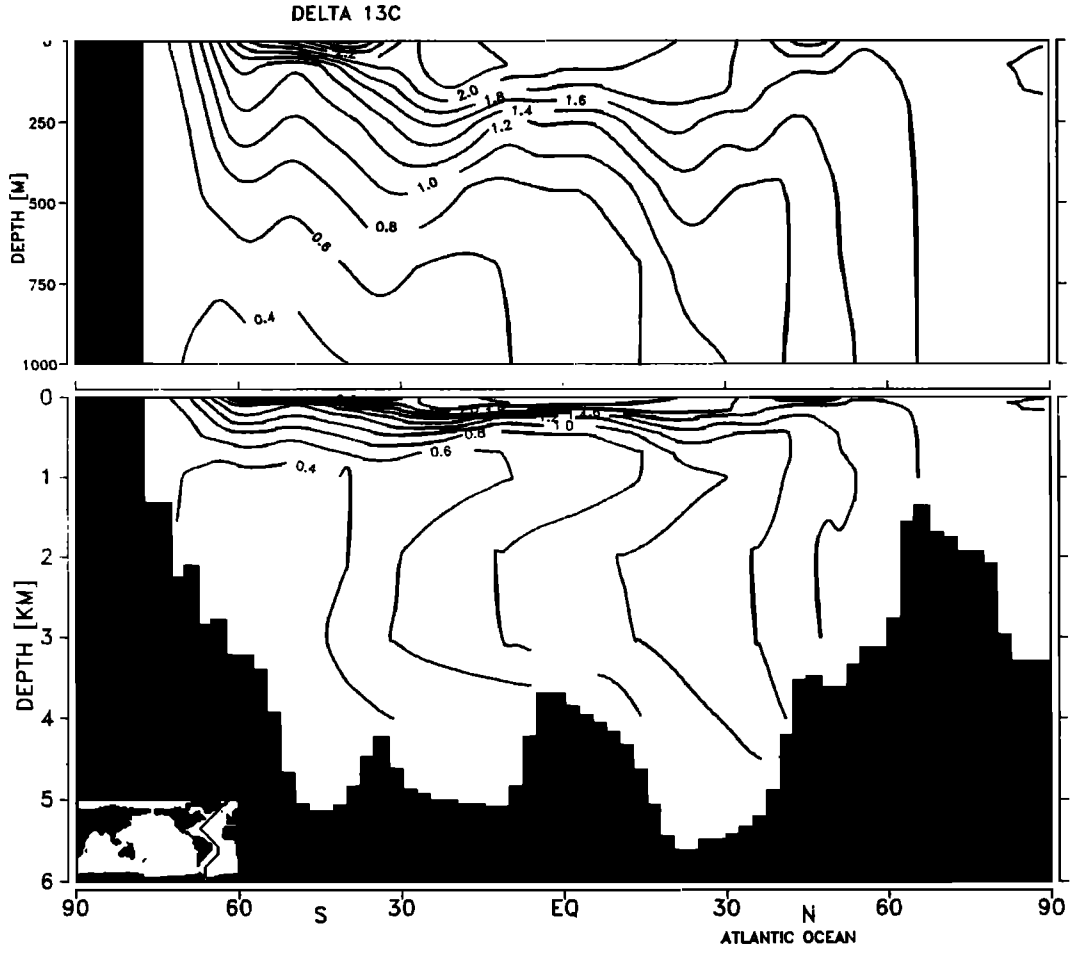

Fig. 13. $\delta^{13}C$ of $\sum CO_2$ (in per mil) of the ventilation change run in a cross section close to the position of the Western Atlantic GEOSECS section.

the intercept of the critical $[CO_3^{2-}]$ depth profile [Broecker and Takahashi, 1978] and the modeled vertical $[CO_3^{2-}]$ profile. If blobs of undersaturated water appeared in the upper water column, only the lowermost transition zone between dissolution and preservation of calcite was determined.

3.2. *Comparison With Mean Observations for the Period 18–65 kyr B.P.*

During 18-65 kyr B.P. the Vostok ice core pCO_2 time series shows the strongest reduction of atmospheric CO_2 during the last climatic cycle [Barnola et al., 1987]. The differences between the ice age tracer values and the observed data of the preindustrial situation were averaged over this time interval 18-65 kyr B.P. and compared to the corresponding results for the different sensitivity studies. The comparisons are summarized in Table 6 and Figure 18. In a separate investigation the simultaneous fit of a linear response model to ice core pCO_2 and $\Delta\delta^{13}C$ data proved to be better for the benthic *Cibicidoides* records than for the *Uvigerina* data. For direct comparison with the single experiments only the more reliable benthic $\delta^{13}C$ records based on *Cibicidoides* $CaCO_3$ shell material were considered.

The observed data pattern (Figure 18, Table 6) shows the strong glacial pCO_2 reduction, a marked increase in the $\Delta\delta^{13}C_{p-b}$ values in equatorial Pacific and Atlantic waters, and a reduction in the $\Delta\delta^{13}C_{b(Atl)-b(Pac)}$ value compared to preindustrial times, indicating a reduced age contrast between Atlantic and Pacific deep waters. For the calcite lysocline depth changes, reversed

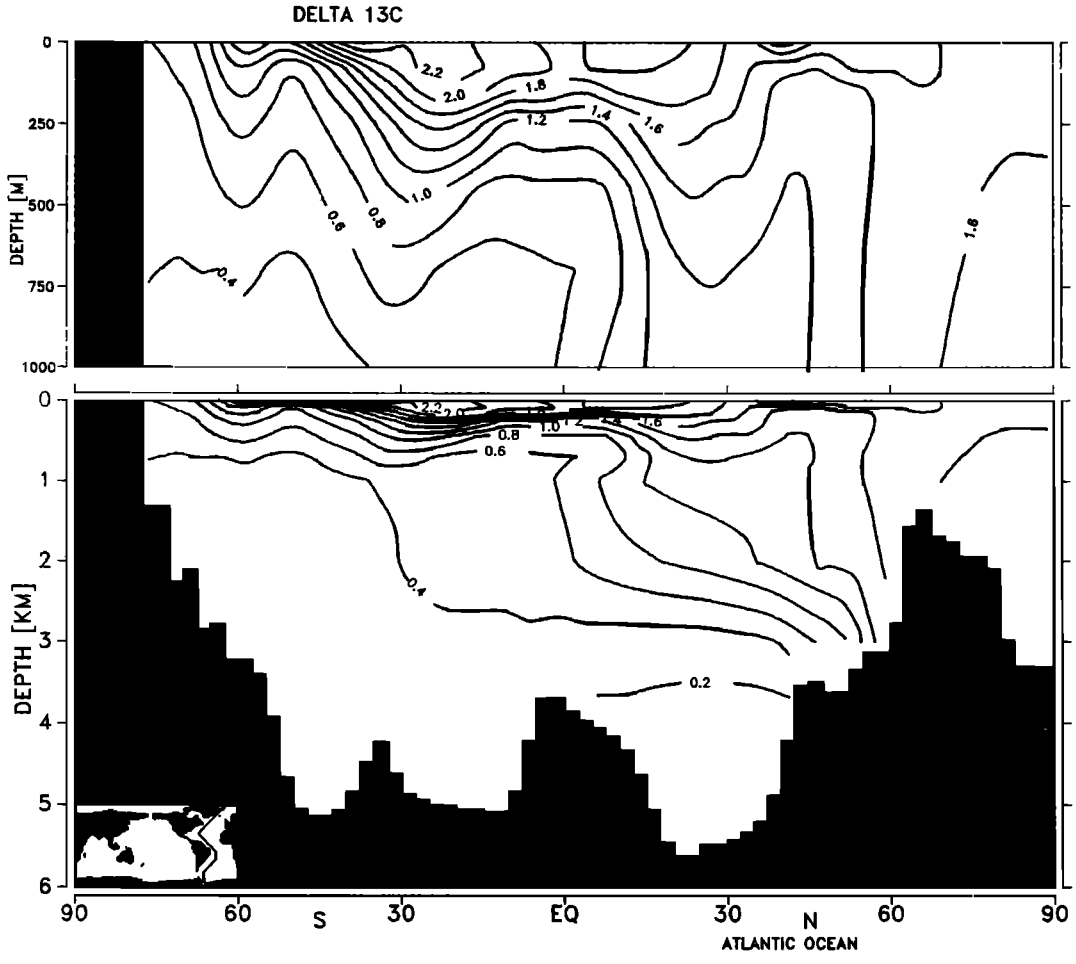

Fig. 14. $\delta^{13}C$ of $\sum CO_2$ (in per mil) of the advective pattern change run (second stable mode) in a cross section close to the position of the Western Atlantic GEOSECS section.

trends are observed for the Atlantic and the Indian plus Pacific oceans: a shallowing in the Atlantic and a deepening in the Indian and Pacific.

The productivity and nutrient cycle experiments (high-latitude productivity, Redfield ratio, PO_4/POC inventory) all show increased $\Delta\delta^{13}C_{p-b}$ values. There is also good agreement with the Pacific Ocean lysocline shift, in contrast to that of the Indian and NW Atlantic oceans. The Redfield ratio and the POC inventory scenarios show the highest qualitative consistency with observed data. The difference between the PO_4 inventory and the Redfield ratio scenario seen in the change of the NW Atlantic lysocline depth level is probably due to the additional change in alkalinity during biomass production in the Redfield ratio experiment. (Though not explicitly modeled, the effect of a changed nitrate consumption with a changed Redfield ratio is accounted for in the model.)

As expected from the negligible fractionation of carbon isotopes for $CaCO_3$ production, the $CaCO_3$ cycle experiments ($CaCO_3$ inventory, rain ratio) yield smaller changes in the $\delta^{13}C$ records than most of the nutrient cycle experiments. These experiments cannot explain the decreasing pCO_2 parallel to the decreasing contrast in $\Delta\delta^{13}C_{b(Atl)-b(Pac)}$ during glaciation. Furthermore, the result of the rain ratio scenario contradicts the interglacial-glacial trends for all lysocline depth level records. The $CaCO_3$ inventory change yields qualitatively correct lysocline shifts in the Indian and Pacific oceans. The shallowing of the lysocline depth level in the Indian and Pacicfic oceans for the rain ratio scenario can be readily explained by the reduced $CaCO_3$

flux to the deep water and the corresponding lower $CaCO_3$ saturation in the deep layers below the high-fertility regions of the central Pacific. However, the increase in calcite saturation

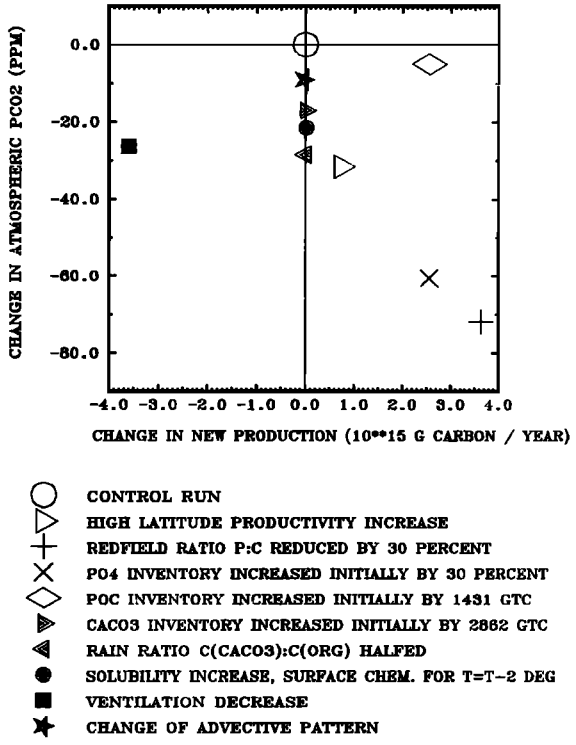

Fig. 15. Results of the sensitivity studies. Deviations in atmospheric CO_2 partial pressure (in parts per million) versus deviations in POC new production (in GtC/yr = 10^{15} g carbon per year) from the reference run.

for a decrease in $CaCO_3$ production in the North Atlantic is at first sight surprising. It is caused by the direct transfer of carbonate ions to the deep water by deep-water production in the sub-Arctic North Atlantic. This alternative path of injecting CO_3^{2-} into deep layers is more efficient than the normal route of calcite production in surface waters, sinking of the aggregates through the water column, and subsequent dissolution in undersaturated regions.

For the solubility pump or sea surface reduction experiment the tracer changes are comparatively small. Qualitative agreement between observed and modeled changes is achieved only for the $\Delta\delta^{13}C_{p-b}$ signals and the Indian Ocean lysocline.

The sensitivity experiments involving changes in the velocity field (change in ventilation or advective pattern) both show a reduction of CO_2 partial pressure in the atmosphere but also reveal distinct changes in tracer patterns. The ventilation reduction experiment shows qualitative agreement with observed changes only for the $\Delta\delta^{13}C_{p-b}$ shift in the Pacific and the Indian Ocean lysocline. In contrast, the experiment with a change in the advective pattern reproduces all tracer changes qualitatively, with the exception of the Pacific $\Delta\delta^{13}C_{p-b}$ change.

Table 7 summarizes the results of all sensitivity experiments. Results which are in qualitative agreement with the observations are represented by a "+", those contradicting the observations with a "–". It is found that none of the sensitivity experiments alone is able to reproduce the complete tracer pattern observed for average glacial

TABLE 1. Absolute Values of Sensitivity Experiment Results for pCO_2 and POC new production

No.	Scenario	pCO_2, ppm	New production, GtC/yr
0	Control run	278.5	8.99
1	High-latitude productivity increase	246.9	9.73
2	Redfield ratio reduction	206.7	12.62
3	PO_4 inventory increase	217.9	11.55
4	POC inventory increase	273.4	11.55
5	$CaCO_3$ inventory increase	261.5	8.99
6	Rain ratio reduction	250.0	8.99
7	Solubility increase (SST decrease)	257.0	9.00
8	Ventilation reduction	252.2	5.39
9	Change of advective pattern	269.5	8.96

conditions satisfactorily. However, the experiment with a changed ocean circulation regime appears promising and can explain at least qualitatively most of the signatures of the observed features. Better agreement with observations could clearly have been obtained by combining different hypotheses. This will be pursued in a separate study.

4. CONCLUSION

Our sensitivity studies show that simple changes in the biological and chemical parameters of the marine carbon cycle can in principle explain the strong pCO_2 reduction during the last glaciation, but the model results are not consistent with other data from marine sediment cores. A similar statement can be made for the two circulation experiments. A change in the strength of the current velocities (ventilation change), or a change in the structure of the global ocean circulation can both induce an atmospheric pCO_2 reduction, but both experiments fail to reproduce all other observed carbon cycle tracer changes simultaneously. Qualitatively, the switch in the structure of the ocean circulation to the second stable mode yields the best agreement with the observations. However, none of the experiments in isolation can explain the ice core pCO_2 records and the marine ^{13}C and $CaCO_3$ records completely.

The anomaly signature for the experiment with the second stable ocean circulation mode violates the observations qualitatively only for the Pacific $\Delta\delta^{13}C_{p-b}$ signal. However, it yields only 9 ppm reduction in atmospheric CO_2 content, i.e. only

TABLE 2. Differences From the Control Run for Sensitivity Study Experiment Results for pCO_2 and POC New Production

No.	Scenario	pCO_2, ppm	New production, GtC/yr
0	(Control run)	(0.0)	(0.0)
1	High-latitude produtivity increase	−31.6	+0.74
2	Redfield ratio reduction	−71.8	+3.63
3	PO_4 inventory increase	−60.6	+2.56
4	POC inventory increase	−5.1	+2.56
5	$CaCO_3$ inventory increase	−17.0	0
6	Rain ratio reduction	−28.5	0
7	Solubility increase (SST decrease)	−21.5	+0.01
8	Ventilation reduction	−26.3	−3.60
9	Change of advective pattern	−9.0	−0.03

TABLE 3. Sediment Cores That Were Used for the Comparison With the Modeled $\delta^{13}C$ Values

Identification	Author(s)	Core(s)	Position	Water Depth, m
1	Shackleton and Pisias [1985]	V19-30	03°23'S 83°21'W	3091
2	Shackleton et al. [1983]	V19-30	03°23'S 83°21'W	3091
3	Winn (unpubl. data, 1990)	Sonne 12-98	10°32'S 109°45'W	3371
4	Curry and Crowley [1987]	"stacked record" of		
		EN066-38GGC	04°55'N 20°30'W	2931
		13519	05°40'N 19°51'W	2862
		KNR110-43PC	04°43'N 43°39'W	3436
		KNR110-82GGC	04°20'N 43°29'W	2816
		DSDP 502B	11°29'N 79°23'W	3051
5	Sarnthein et al. [1984]	13519	05°40'N 19°51'W	2862
6	Zahn et al. [1986]	13519	05°20'N 19°51'W	2862
7	Shackleton [1977]	12392	25°10'N 16°51'W	2575

TABLE 4. The $\delta^{13}C$ Records From Marine Sediment Cores That Have Been Compiled for Comparison With Model Results

Record Identification	Record Type	Location	Foraminifera Species	Error Estimate, per mil
1	$\Delta\delta^{13}C_{p-b}$	Pacific	planktonic Neogloboquadrina dutertrei benthonic Uvigerina senticosa	+/- 0.057
1, 3	$\Delta\delta^{13}C_{p-b}$	Pacific	planktonic Neogloboquadrina dutertrei benthonic Cibicidoides wuellerstorfi	+/- 0.064
4	$\Delta\delta^{13}C_{p-b}$	Atlantic	planktonic Globigerinoides sacculifer benthonic Uvigerina senticosa	(+/- 0.15)
5, 6	$\Delta\delta^{13}C_{p-b}$	Atlantic	planktonic Globigerinoides sacculifer benthonic Cibicidoides wuellerstorfi	+/- 0.071
2, 7	$\Delta\delta^{13}C_{b(Atl)-b(Pac)}$	Atlantic minus Pacific	Atlantic Uvigerina peregrina, Planulina wuellerstorfi, Melonis pompilloides Pacific Uvigerina senticosa	+/- 0.13
3, 5	$\Delta\delta^{13}C_{b(Atl)-b(Pac)}$	Atlantic minus Pacific	Cibicidoides wuellerstorfi	+/- 0.071

See Table 3 for record identification numbers.
Parentheses around error estimate value indicates that estimate includes dating error.

10 % of the observed reduction during glaciation. A weak "nutricline" appears in the North Atlantic (Figure 14), reproducing in part the fractionation of the nutrient inventories between surface plus intermediate waters and deep water deduced from the observed $\delta^{13}C$ and Cd/Ca distribution [Boyle, 1988].

The ventilation change experiment for the Pacific Ocean leads to a stronger reduction of atmospheric pCO_2 (-26 ppm). However, in this experiment the nutrient or $\delta^{13}C$ contrast between upper and deeper waters is not marked by a "nutricline" between intermediate and deep layers (Figure 13). The Atlantic $\delta^{13}C$ pattern (Figure 13) is in fact very similar to the control run. It appears that both circulation fields, ventilation change and change of advective pattern (second stable mode) alone, cannot reproduce the real situation during the last glaciation. However, a combination of a circulation mode intermediate between the advective pattern change scenario and the ventilation change scenario is promising. By slowing down the second stable mode velocity field, an improved simulation of the Pacific $\Delta\delta^{13}C_{p-b}$ increase and a further reduction of atmospheric pCO_2 can be expected. However, a decrease of the glacial atmosphere pCO_2 level of 80 ppm by this circulation change still appears questionable.

Due to the comparatively high resolution of the model used in this study, any measurement of any oceanic palaeoclimate tracer will be of use to support further investigations as an additional constraint. In general, it would be desirable to have observational data that fulfil the following requirements: high signal/noise ratio, representativeness, and linear independency from one another. In addition to the fairly large data base for $\delta^{13}C$ and calcite saturation data, sources of separate information about the physical and biogeochemical status of the ocean would be useful. As can be seen from our sensitivity experi-

TABLE 5. Sediment Cores That Provide the Basis for the Comparison of the Calcite Lysocline Depth Level Between Model and Observations

Lysocline Depth Record	Author(s)	Core(s)	Position
Indian Ocean	Peterson and Prell [1985]	V34-55	06°02'S 88°57.4'E
		V34-54	06°05'S 89°10'E
		V34-48	06°15'S 90°33'E
		V34-53	06°07'S 89°35'E
		V34-52	06°10'S 89°48'E
		V34-49	06°22'S 90°36'E
		V34-51	06°11'S 89°58'E
Pacific Ocean	Farrell and Prell [1989]	V24-55	02°03'N 134°38'W
		W8402A-14GC	00°57'N 138°57'W
		DSDP hole 573A	00°30'N 133°19'W
		SDSE59	03°05'N 133°06'W
		RC11-209	03°39'N 140°04'W
		RC11-210	01°49'N 140°03'W
		PLDS 130 and 131	04°00'N 136°00'W
		V24-58	02°16'N 141°40'W
		V28-179	04°37'N 139°36'W
		SDSE60	01°35'N 134°57'W
		DSDP hole 574	04°13'N 133°20'W
		V24-59	02°34'N 145°32'W
		RC12-66	02°37'N 148°13'W
		V24-62	03°04'N 153°35'W
		RC12-65	04°39'N 144°58'W
		RC12-63	05°58'N 142°39'W
NW Atlantic	Balsam [1983]	A164-44	33°57'N 62°39'W
		A173-4	33°52'N 62°32'W
		E2D-79-1	34°28'N 63°55'W
		E2D-79-2	33°55'N 62°33'W
		E2D-79-3	33°24'N 61°40'W
		E2D-79-9	33°26'N 61°31'W
		E2D-79-12	33°24'N 61°37'W
		E2D-79-15	33°22'N 62°30'W
		E2D-79-16	33°23'N 62°38'W
		E2D-79-17	33°26'N 62°29'W
		E2D-79-24	33°36'N 62°20'W
		E2D-79-30	33°35'N 62°23'W
		E2D-79-31	33°55'N 62°42'W
		RC8-145	33°35'N 62°23'W
NE Atlantic	Crowley [1983]	V23-100	21°18'N 22°41'W
		A180-32	29°07'N 26°15'W
		(V26-41)	(19°19'N 26°08' W)
		(V27-171)	(21°44'N 32°34' W)
		(V26-37)	(16°38'N 31°06' W)
		(A180-39)	(25°50'N 19°18' W)

Parentheses indicate that the information from those cores was used only for calibration.

ments, calcite saturation and $\delta^{13}C$ are influenced approximately to an equal extent by biogeochemical parameters and the oceanic field of motion. We consider a better radiocarbon data coverage for the glacial ocean over the last 120 kyr B.P. to be the most useful additional information that is goverened primarily by the circulation. This time interval is necessary to consider also the early stages of the glaciation. Critical regions would be the deep-water production areas in the North Atlantic, the combined upwelling and deep convection regimes of the Southern Ocean, the

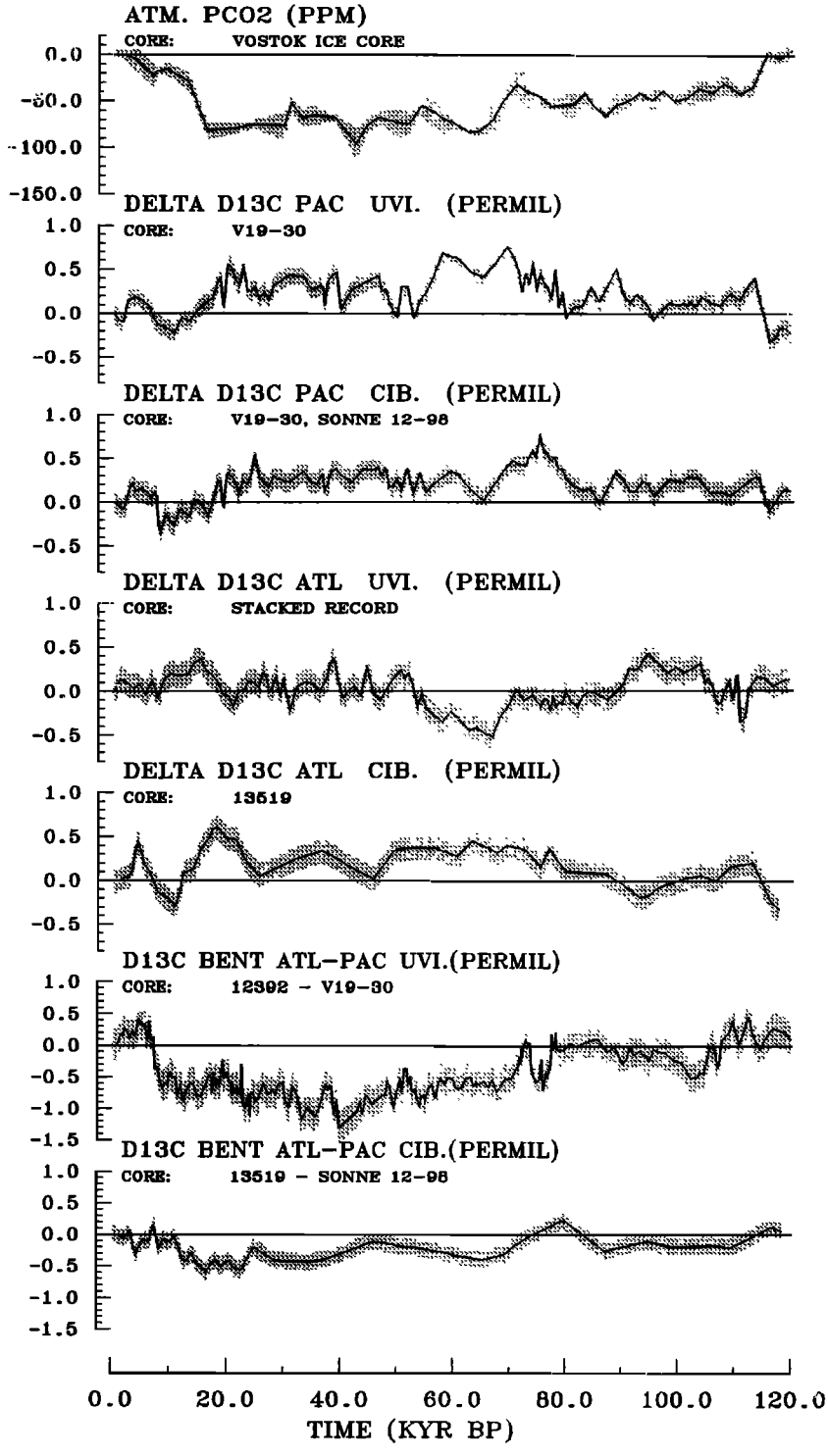

Fig. 16. Ice core and marine ^{13}C sediment core records that were considered for comparison with model results (cf. Table 4). The shaded areas indicate the error estimate (see text). Only *Cibicidoides* based records (CIB.) were directly used for comparison with model results. Curves based on *Uvigerina* shell material (UVI.) are shown for illustration of the differences from the *Cibicidoides* records.

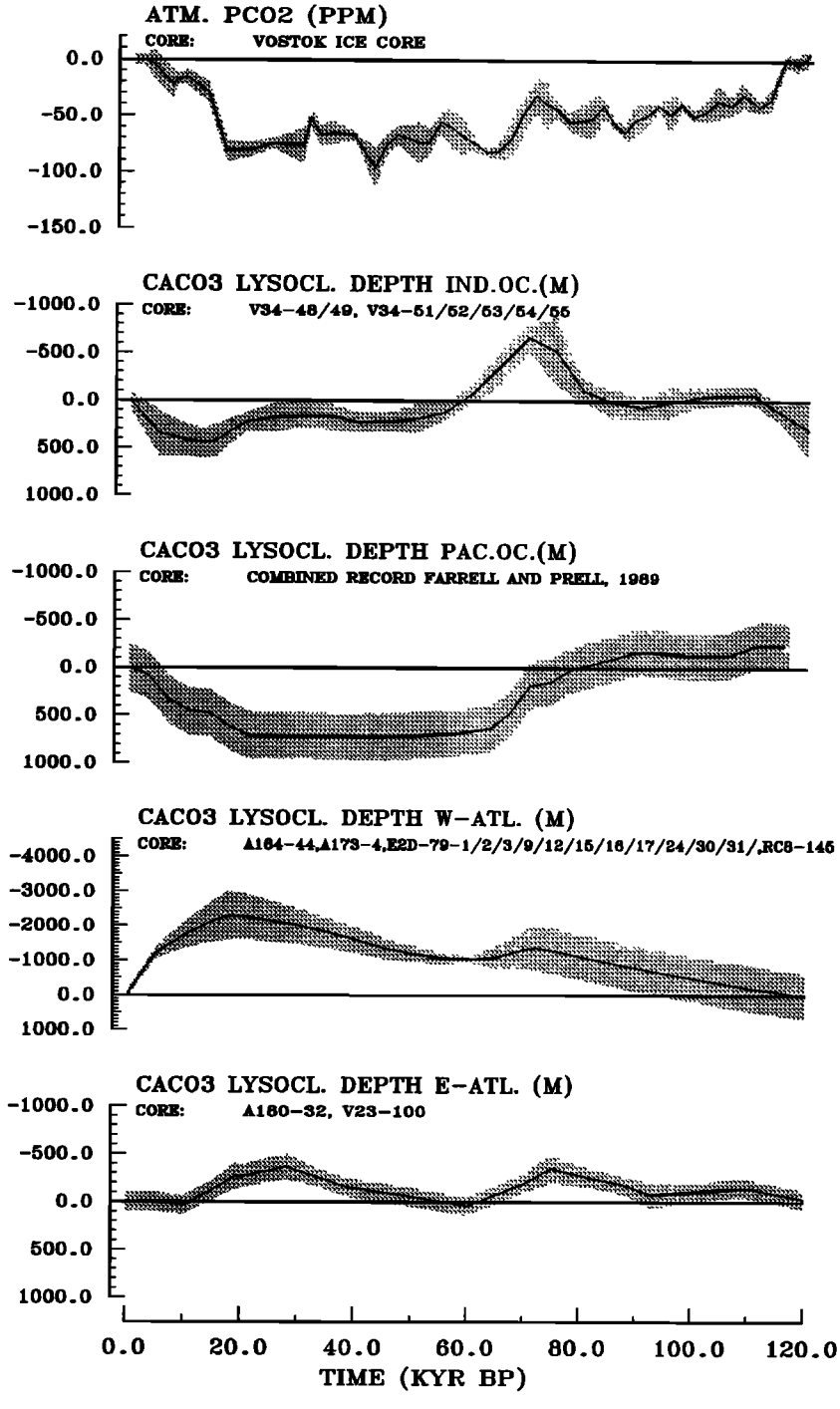

Fig. 17. Ice core and marine $CaCO_3$ saturation (lysocline depth) sediment core records as used for comparison with model results (cf. Table 5). The shaded areas indicate the error estimate (see text).

TABLE 6. Comparison of Observations for the Period 18–65 kyr B.P., and Model Results for the Different Sensitivity Experiments

No.	Scenario	pCO_2, ppm	$\Delta\delta^{13}C_{p-b}$, Pacific, per mil	$\Delta\delta^{13}C_{p-b}$ Atlantic, per mil	$\Delta\delta^{13}C_{b(Atl)-b(Pac)}$, per mil	Lysocline Depth, m			
						Indian	Pacific	NW Atlantic	NE Atlantic
0	Observation	−72.5	0.26	0.28	−0.31	130	696	−1589	−155
1	High-latitude productivity increase	−31.6	0.13	0.20	0.00	−192	103	54	33
2	Redfield ratio reduction	−71.8	0.38	0.95	−0.16	−772	1423	−10	−173
3	PO_4 inventory increase	−60.6	0.29	0.68	−0.08	−679	876	36	−65
4	POC inventory increase	−5.1	0.14	0.44	−0.13	−1726	457	−253	−380
5	$CaCO_3$ inventory increase	−17.0	0.00	0.02	−0.01	835	695	x 341	505
6	Rain ratio reduction	−28.5	0.07	0.04	0.05	−1143	−653	119	36
7	Solubility increase	−21.5	0.02	0.03	0.01	39	−113	52	26
8	Ventilation reduction	−26.3	0.09	−0.13	0.06	8	−383	81	128
9	Change of advective pattern	−9.0	−0.08	0.21	−0.38	209	470	−1252	−655

An x preceding a value indicates that it was extrapolated from run with 1/6 of the anomaly.

TABLE 7. Comparison of Observations for the Period 18–65 kyr B.P., and Model Results for the Different Sensitivity Experiments in a Qualitative Sense

No.	Scenario	pCO_2, ppm	$\Delta\delta^{13}C_{p-b}$, Pacific, per mil	$\Delta\delta^{13}C_{p-b}$ Atlantic, per mil	$\Delta\delta^{13}C_{b(Atl)-b(Pac)}$, per mil	Lysocline Depth, m			
						Indian	Pacific	NW Atlantic	NE Atlantic
0	Observation	−72.5	0.26	0.28	−0.31	130	696	−1589	−155
1	High-latitude productivity increase	+	+	+	−	−	+	−	−
2	Redfield ratio reduction	+	+	+	+	−	+	+	+
3	PO_4 inventory increase	+	+	+	+	−	+	−	+
4	POC inventory increase	+	+	+	+	−	+	+	+
5	$CaCO_3$ inventory increase	+	−	+	+	+	+	−	−
6	Rain ratio reduction	+	+	+	−	−	−	−	−
7	Solubility increase	+	+	+	−	+	−	−	−
8	Ventilation reduction	+	+	−	−	+	−	−	−
9	Change of advective pattern	+	−	+	+	+	+	+	+

Qualitative agreement between model results and observations is indicated by "+", discrepancies are indicated by "−".

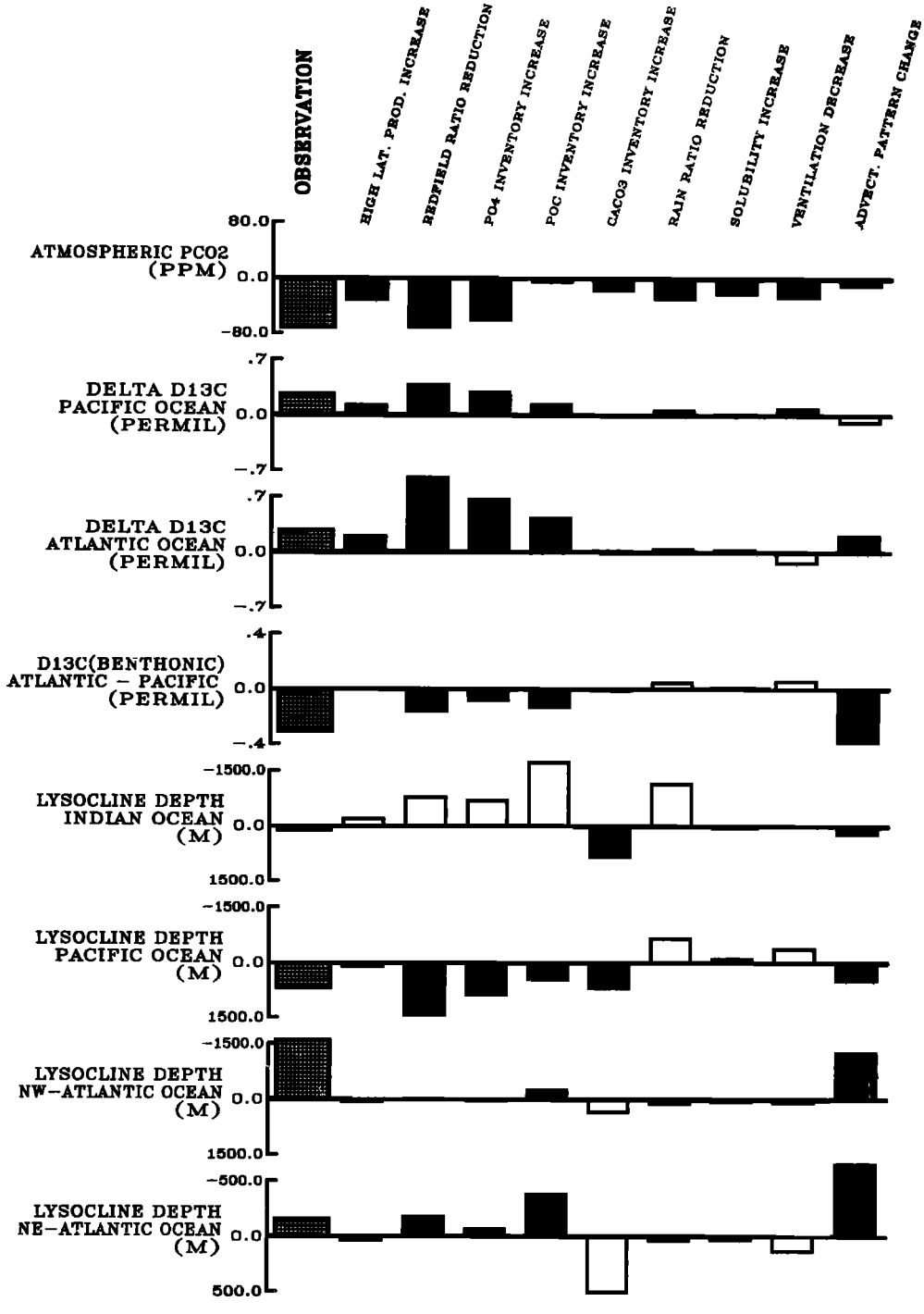

Fig. 18. Results of the sensitivity studies. The bars in the left column denote the observed average tracer change for the 18–65 kyr B.P. interval. The solid areas represent the modeled changes in tracer distributions resulting from the different sensitivity experiments that are in qualitative agreement with the observations.

North Pacific, and all equtorial upwelling areas. In order to produce more realistic oceanic model velocity fields for the glacial ocean a very detailed ice age surface salinity field and also glacial wind stress data (both as global data sets) are necessary. When the ice age circulation can once be fixed by these data, the carbon cycle data provide a further basis to constrain this model result. On the other hand, the effect of a separate change of biogeochemical parameters could probably be estimated from the residual of the $\delta^{13}C$ and $CaCO_3$ saturation observations and a carbon cycle model run with a realistic ice age ocean velocity field. The effect of a primarily ecologic change, i.e., a change in the chemical and biological parameters of the carbon cycle, could potentially be decisive for an understanding of the glacial pCO_2 drawdown. Also for the carbon cycle tracers, three-dimensional global data sets would be most useful to constrain the model results. As the lysocline depth level provides important independent information, the latitudinal variation of this parameter at least for one cross section through each of the Atlantic, Indian, and Pacific oceans would be most useful. For the North Atlantic, it turns out that a considerable scatter exists for the reaction of the oceanic biogeochemical system on changes in physical as well as ecological parameters between the eastern and western part. Therefore both sides of at least the Atlantic Ocean must be documented thoroughly by paleoclimatic observations besides the other critical regions that are listed above in the radiocarbon data discussion.

For further investigations it is thus essential to compile a more detailed consistent proxy record data base. The simplification in considering only global changes in the carbon cycle parameters should be abandoned in further studies. A regional differentiation of the carbon cycle parameters should be introduced into the model, if the parameters can be firmly established as functions of fertility and hydrographic conditions.

The development of marine velocity fields for glacial conditions seems to be the most promising effort toward explaining the glacial pCO_2 reduction and the corresponding climatic impact.

The results of this study should be considered as a first step. As the most prominent parameter changes appear to have taken place around 70 kyr B.P., preceding the period of strongest pCO_2 reduction, glacial ocean studies should concentrate on the corresponding events with at least the same emphasis as spent on termination I.

APPENDIX: MODEL DETAILS

Gas Exchange Ocean/Atmosphere

Gas exchange between ocean and atmosphere is performed with a simple bulk formula:

$$F = \lambda \cdot (pCO_2(\text{air}) - pCO_2(\text{water}))$$

where F is the gas exchange flux and λ is the gas exchange coefficient. For λ a value of 19 mol m^{-2} yr^{-1} at 270 ppm is adopted [cf. Broecker et al., 1986].

Tracer Advection and Biological Productivity

All tracers are transported with the ocean velocity field. An upstream formulation of the tracer equation (continuity equation for amount of matter) is applied:

tracer equation

$$\frac{dc}{dt} = -\text{div}(\vec{v} \cdot c) - q$$

upstream formulation

$$\frac{c^{t+\Delta t} - c^t}{\Delta t} = -\sum_i v_i \frac{c_i^{t+\Delta t} - c^{t+\Delta t}}{\Delta x_i} - a \cdot I_l \cdot \frac{V_{max} \cdot (c^{t+\Delta t})^2}{K_s + c^{t+\Delta t}} \quad (1)$$

where

c: tracer concentration

$\vec{v}$: velocity vector

q: term for sources and sinks

v_i: velocity component in the direction of grid point i

Δx_i: distance to neighboring grid point i

c_i: tracer concentration at neighboring grid point i

a: 1 if c is nutrient concentration in the surface layer, 0 otherwise

I_l: light factor (dependent on latitude)

V_{max}: maximum velocity of nutrient uptake

K_s: half saturation constant (PO_4 concentration, where $dc/dt = c \cdot V_{max}/2$)

Uptake of PO_4 as biolimiting nutrient by phytoplankton in the surface layer is the only additional process included in the tracer transport equation (second term on the right-hand side of (1)). The advection equation is solved iteratively by a single-level scheme. Uptake of nutrients by organisms is included in this equation to allow a shorter time constant for phytoplankton growth compared to the time step of 1 year. All the other chemical interactions are calculated in separate routines (time splitting method).

The biological POC production is assumed to follow Michaelis-Menten kinetics for nutrient uptake (e.g. Parsons and Takahashi, 1973). For the light factor I_l the same latitudinal profile as in Bacastow and Maier–Reimer (1990) is used. It is coherent with the latitudinal distribution of the annual sum of solar radiation incident on the ocean surface layer (Figure A1). The latitudinal profile for the light factor I_l as prescribed in the sensitivity experiment with an increase of biological productivity at high latitudes is given in Figure A2. For uptake of inorganically dissolved carbon by phytoplankton a Redfield ratio of P:C = 1:122 [Takahashi et al., 1985] is prescribed.

$CaCO_3$ production is set proportional to the production of POC according to the rain ratio (C_{CaCO3}:$C_{organic}$) chosen. A maximum of 1:4 is used with strong reduction of calcite production (close to zero) at temperatures below 2°C (Figure A3).

Particle Flux Through the Water Column

Biogenic particulate matter is produced only in the uppermost model layer and is immediately redistributed within the water column in amounts decreasing with depth. The immediate redistribution is a reasonable assumption, because the time scale for the particles sinking through the water column is shorter (about 100 m/day [e.g., Suess, 1980]) than the time step of 1 year. 20% of the $CaCO_3$ production is assumed to fall immediately to the bottom layer, while the remainder is distributed according to an exponentially decreasing vertical flux:

$$F_{CaCO3}(z) = (P_{CaCO3} - S_{CaCO3}) \cdot \exp(\frac{-z}{d_p}) + S_{CaCO3}$$

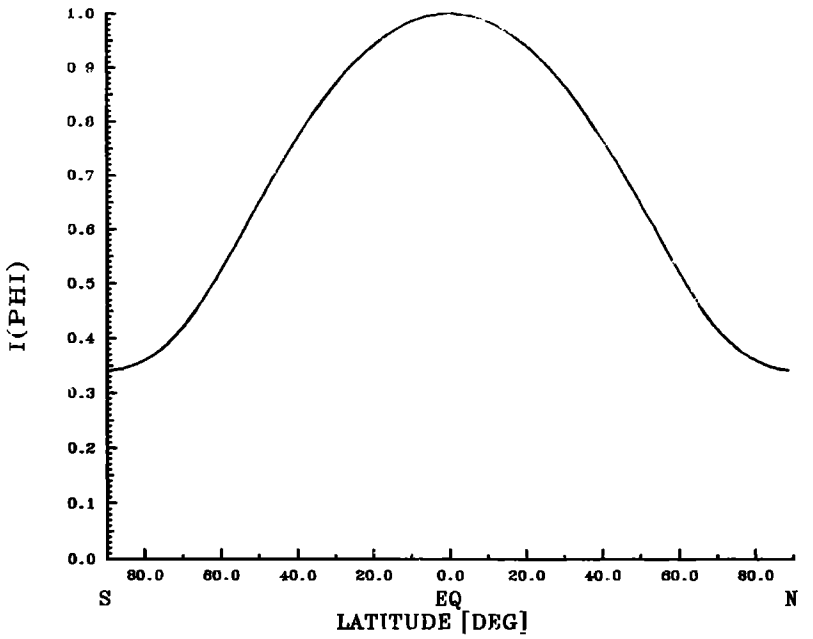

Fig. A1. Latitudinal profile for the light factor I_l, which is used for the parameterization of the growth conditions for phytoplankton (control run).

where

z: depth

P_{CaCO3}: annual production of $CaCO_3$

S_{CaCO3}: part of P_{CaCO3} that sinks immediately to the bottom layer (here 20%)

d_p: e-folding-depth for $CaCO_3$ flux (here 4000 m)

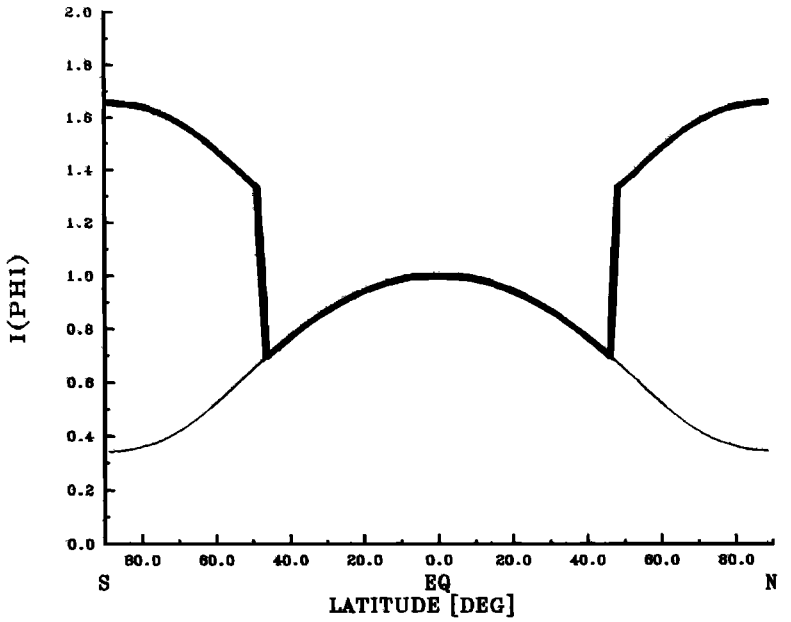

Fig. A2. Latitudinal profile for the light factor I_1, that is used for the parameterization of the growth conditions for phytoplankton as prescribed in the sensitivity experiment with an increase of biological productivity at high latitudes (heavy line) (light line: control run values).

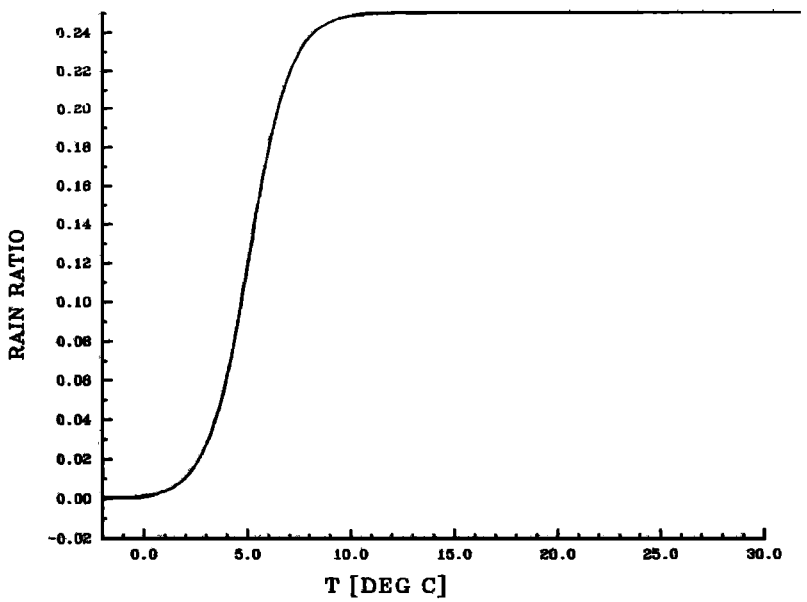

Fig. A3. Temperature dependency for the rain ratio C_{CaCO3}:$C_{organic}$ as used in the model.

By this formulation of the vertical redistribution of newly formed $CaCO_3$ no degradation of $CaCO_3$ is included yet, that is performed separately in another step (see below).

POC flux is assumed to follow the 1/z-law after Suess [1980], with a modification of distributing about one third of the POC new production (28.7% = $P_{POC} - F_1(50\,m)$, see below) like the newly formed $CaCO_3$. This addition is introduced to account for organic material coated by hard shells:

$$F_{POC} = F_1 + F_2$$

with

$$F_1 = \frac{P_{POC}}{0.0238 \cdot z + 0.212}$$

$$F_2 = (P_{POC} - F_1(50\,m) - S_{POC}) \cdot \exp(\frac{-z}{d_p}) + S_{POC}$$

where

z: depth

P_{POC}: annual production of POC

S_{POC}: part of P_{POC} that sinks immediately to the bottom layer (here 5.7%; that is 20% of those 28.7% of total POC produced that are not considered by the 1/z-formulation of Suess [1980])

d_p: e-folding-depth for $CaCO_3$ flux (here 4000 m)

Dissolution of $CaCO_3$ Particles

Degradation of $CaCO_3$ is controlled by the degree of undersaturation of seawater with respect to calcite. The destruction of aragonite (the metastable modification of marine $CaCO_3$) is accounted for in the model by allowing partial destruction of $CaCO_3$ even in cases of calcite supersaturation. After the vertical redistribution of newly produced $CaCO_3$ particles, at first the deviation ΔCO_3 from the saturation concentration is calculated. (Since in seawater the calcium concentration is almost constant and much higher than the CO_3^{2-} concentration, the marine $CaCO_3$ saturation is almost entirely determined by the amount of CO_3^{2-} ions in solution.) Then the amounts of total $CaCO_3$ available in the respective grid box that are dissolved (D_{pot}) or can be precipitated (E) are determined and the concentrations for $\sum CO_2$ and $CaCO_3$ at the new time level are accordingly:

$$\Delta CO_3 = \left[CO_3^{2-}\right]^t - \left[CO_3^{2-}\right]_{sat}$$

$$D_{pot} = [CaCO_3]^t \cdot 0.5 \cdot (1 - \frac{\Delta CO_3}{c_1 + |\Delta CO_3|})$$

$$E = \max(0, \Delta CO_3)$$

$$\left[\sum CO_2\right]^{t+\Delta t} = \left[\sum CO_2\right]^t + D_{pot} - c_2 \cdot E$$

$$[CaCO_3]^{t+\Delta t} = [CaCO_3]^t - D_{pot} + c_2 \cdot E$$

where

ΔCO_3: deviation of carbonate concentration from the saturation value

$\left[CO_3^{2-}\right]^t$: carbonate concentration at old time level

$\left[CO_3^{2-}\right]_{sat}$: saturation concentration of carbonate

D_{pot}: amount of $CaCO_3$ that reenters solution

E: amount of $CaCO_3$ that can be precipitated

$[\sum CO_2]$: total dissolved inorganic CO_2 at new and old time levels respectively

$[CaCO_3]$: calcium carbonate concentration at new and old time levels respectively

c_1, c_2: adjustable constants (here $c_1 = 10^{-4}$ μmol/L, $c_2 = 1$ in bottom layer and zero else)

Remineralization of Organic Matter

Remineralization of organic matter and corresponding oxygen consumption are modeled according to a fixed Redfield ratio P:ΔO_2 of 1:–172 [Takahashi et al., 1985]. O_2 concentration is not allowed to become negative. In the case of full O_2 consumption, POC degradation stops at the respective grid point. After the determination of

the amount of POC that is remineralized during one time step (ΔPOC) the POC, PO_4, and O_2 concentrations for the new time level are calculated:

$$\Delta POC = r \cdot \min(([O_2]_{min} - [O_2]^t) \cdot R_{Red}, [POC]^t)$$

$$[POC]^{t+\Delta t} = [POC]^t - \Delta POC$$

$$[PO_4]^{t+\Delta t} = [PO_4]^t + \Delta POC$$

$$[O_2]^{t+\Delta t} = [O_2]^t - \frac{\Delta POC}{R_{Red}}$$

where

ΔPOC: amount of POC that can be remineralized during one time step

r: remineralization rate (here 1.0 $year^{-1}$ in the surface layer, 0.05 $year^{-1}$ elsewhere)

R_{Red}: Redfield ratio P:ΔO_2

$[O_2]$: oxygen concentration at the new and old time step respectively

$[O_2]_{min}$: threshold value of oxygen concentration for bacterial decomposition

$[PO_4]$: phosphate concentration at the new and old time step respectively (normalized to a POC concentration by the Redfield ratio P:C)

[POC]: particulate organic carbon concentration at the new and old time step respectively

Interaction Between Water Column Concentrations and Sediment

$CaCO_3$ and POC are allowed to enter the sediment pool in an amount proportional to their concentration in particulate form in the bottom layer. This step is carried out after the remineralization (POC) and dissolution ($CaCO_3$) steps. The system is closed by resuspension of sedimented matter into the bottom layer at a fixed rate proportional to the sediment content of the respective grid cell. Resuspension occurs in reality due to bioturbation in the uppermost sediment.

Inorganic Carbon Chemistry

For the inorganic carbon chemistry relations (see summary by Maier-Reimer and Hasselmann [1987]) the dissociation constants for carbonic and boric acid, K_1, K_2, and K_B, are taken from Mehrbach et al. [1973], and Edmond and Gieskes [1970], with pressure dependency according to Culberson and Pytkowicz [1968]. The solubility coefficients for CO_2 and O_2 are adopted from Weiss [1974] and Weiss [1970]. The apparent $CaCO_3$ solubility product is used here exclusively for calcite, making use of the formulations of Ingle [1975] with corrections for hydrostatic pressure after Edmond and Gieskes [1970].

Acknowledgments. We are grateful to K. Hasselmann for his many ideas that have found their way into this paper. Thanks are due to M. Sarnthein, M. Heimann, A. Spitzy, and V. Ittekkot for many fruitful discussions. The velocity fields in the carbon cycle model were kindly provided by U. Mikolajewicz. T. Tönsing and M. Boettinger compiled the cross section plot software. The reviewer and the associate editor helped us with their suggestions for making the manuscript easier to read. This work was supported by the Bundesministerium für Forschung und Technologie (BMFT contract 07KF2121, Globale Klimamodelle, and 07KF0214, Marine Paläoklimatologie) and the Commission of the European Communities (contracts EV4C-0030-D and EV4C-0034-D).

REFERENCES

Altenbach, A. V., and M. Sarnthein, Productivity record in benthic foraminifera, in *Productivity in the Ocean: Present and Past*, edited by W. H. Berger, V. S. Smetacek, and G. Wefer, pp. 255-269, John Wiley, New York, 1989.

Bacastow, R. B. and E. Maier-Reimer, Circulation model of the oceanic carbon cycle, *Clim. Dyn.*, *4*, 1990.

Baes, C. F., Jr., Effects of ocean chemistry and biology on atmospheric carbon dioxide, in *Carbon Dioxide Review 1982*, edited by W. C. Clarke, pp. 189-204, Oxford University Press, New York, 1982.

Bainbridge, A. E., *GEOSECS Atlantic Expedition*, vol. 1, *Hydrographic Data 1972-1973*, 121 pp., Superintendant of Documents, U.S. Government Printing Office, Washington, D. C., 1981.

Balsam, W. L., Carbonate dissolution on the Muir Seamount (Western North Atlantic): Interglacial/glacial changes, *J. Sediment. Petrol., 53*, 719-731, 1983.

Bard, E., B. Hamelin, R. G. Fairbanks, and A. Zindler, Calibration of the ^{14}C timescale over the past 30,000 years using mass spectrometric U-Th ages from Barbados corals, *Nature, 345*, 405-410, 1990.

Barnola, J. M., D. Raynaud, Y. S. Korotkevich, and C. Lorius, Vostok ice core provides 160,000-year record of atmospheric CO_2. *Nature, 329*, 408-414, 1987.

Berger, W. H., and R. S. Keir, Glacial-Holocene changes in atmospheric CO_2 and the deep-sea record, in *Climate Processes and Climate Sensitivity*, Geophys. Monogr. Ser. vol. 29, edited by J. E. Hansen and T. Takahashi, pp. 337-351, AGU, Washington, D. C., 1984.

Boyle, E. A., The role of vertical chemical fractionation in controlling late Quaternary atmospheric carbon dioxide, *J. Geophys. Res., 93*, 15701-15714, 1988.

Boyle, E. A., and L. Keigwin, North Atlantic thermohaline circulation during the past 20,000 years linked to high-latitude surface temperature, *Nature, 330*, 35-40, 1987.

Broecker, W. S., Ocean chemistry during glacial time, *Geochim. Cosmochim. Acta, 46*, 1689-1705, 1982.

Broecker, W. S., Carbon dioxide circulation through ocean and atmosphere, *Nature, 308*, 602, 1984.

Broecker, W. S., and T.-H. Peng, *Tracers in the Sea*, 690 pp., ELDIGIO Press, Lamont-Doherty Geological Observatory, Columbia University, Palisades, N. Y., 1982.

Broecker, W. S., and T.-H. Peng, Carbon cycle: 1985 - Glacial to interglacial changes in the operation of the global carbon cycle, *Radiocarbon, 28*, 309-327, 1986.

Broecker, W. S., and T.–H. Peng, The role of $CaCO_3$ compensation in the glacial to interglacial atmospheric CO_2 change, *Global Biogeochem. Cycles, 1*, 15–29, 1987a.

Broecker, W. S., and T.–H. Peng, The oceanic salt pump: Does it contribute to the glacial–interglacial difference in atmospheric CO_2 content?, *Global Biogeochem. Cycles, 1*, 251-259, 1987b.

Broecker, W. S., and T.–H. Peng, The cause for the glacial to interglacial atmospheric CO_2 change: A polar alkalinity hypothesis, *Global Biogeochem. Cycles, 3*, 215-239, 1989.

Broecker, W. S., and T. Takahashi, The relationship between lysocline depth and in situ carbonate ion concentration, *Deep-Sea Res., 25*, 65-95, 1978.

Broecker, W. S., D. W. Spencer, and H. Craig, *GEOSECS Pacific expedition*, vol. 3, *Hydrographic data 1973-1974*, 137 pp., Superintendant of Documents, U.S. Government Printing Office, Washington, D. C., 1982.

Broecker, W. S., J. R. Ledwell, T. Takahashi, R. Weiss, L. Merlivat, L. Memery, T.-H. Peng, B. Jähne, and K. O. Münnich, Isotopic versus micrometeorologic ocean CO_2 fluxes: A serious conflict, *J. Geophy. Res., 91*, 10517-10527, 1986.

Broecker, W. S., M. Andree, G. Bonani, W. Wolfli, H. Oeschger, M. Klas, A. Mix, and W. Curry, Preliminary estimates for the radiocarbon age of deep water in the glacial ocean, *Paleoceanography, 3*, 659-669, 1988.

Broecker, W. S., T.–H. Peng, S. Trumbore, G. Bonani, and W. Wolfli, The distribution of radiocarbon in the glacial ocean, *Global Biogeochem. Cycles, 4*, 103-117, 1990.

Bryan, K., High-latitude salinty effects and interhemispheric thermohaline circulations, *Nature, 323*, 301-304, 1986.

CLIMAP Project Members, Seasonal reconstructions of the earth's surface at the last glacial maximum, Map and Chart Ser. MC-36, Lamont-Doherty Geol. Observ. of Columbia Univ., Palisades, N. Y., 1981.

Crowley, T. J., Calcium-carbonate preservation patterns in the central North Atlantic during the last 150,000 years, *Mar. Geol., 51*, 1-14, 1983.

Culberson, C. H., and R. M. Pytkowicz, Effect of pressure on carbonic acid, boric acid and the pH in sea water, *Limnol. Oceanogr.*, 13, 403-417, 1968.

Curry, W. B., and T. J. Crowley, The $\delta^{13}C$ of equatorial Atlantic surface waters: implications for ice age pCO_2 levels, *Paleoceanography, 2*, 489-517, 1987.

Curry, W. B., and G. P. Lohmann, Carbon isotopic changes in benthic foraminifera from the western South Atlantic: Reconstruction of glacial abyssal circulation patterns, *Quat. Res., 18*, 218-235, 1982.

Curry, W. B., J. C. Duplessy, L. D. Labeyrie, and N. J. Shackleton, Changes in the distribution of $\delta^{13}C$ of deep water $\sum CO_2$ between the last glaciation and the Holocene, *Paleoceanography, 3*, 317-341, 1988.

Delmas, R. J., J.-M. Ascencio, and M. Legrand, Polar ice evidence that atmospheric CO_2 20,000 yr BP was 50 % of present, *Nature, 284*, 155-157, 1980.

De Vooys, C. G. N., Primary production in aquatic environments, in *The Global Carbon Cycle*, edited by B. Bolin, E. T. Degens, S. Kempe and P. Ketner, pp. 259-292, John Wiley, New York, 1979.

Duplessy, J.-C., L. Cherrouard, and F. Vila, Weyl's theory of glaciation supported by isotopic study of Norwegian core K11, *Science, 188*, 1208-1209, 1975.

Duplessy, J.-C., N. J. Shackleton, R. G. Fairbanks, L. Labeyrie, D. Oppo, and N. Kallel, Deepwater source variations during the last climatic cycle and their impact on the global deepwater circulation, *Paleoceanography, 3*, 343-360, 1988.

Dymond, J., and M. Lyle, Flux comparisons between sediments and sediment traps in the eastern tropical Pacific: Implications for CO_2 variations during the Pleistocene, *Limnol. Oceanogr., 30*, 699-712, 1985.

Edmond, J. M., and J. M. T. M. Gieskes, On the calculation of the degree of saturation of sea water with respect to calcium carbonate under in situ conditions, *Geochim. Cosmochim. Acta, 34*, 1261-1291, 1970.

Eppley, R. W., and B. J. Peterson, Particulate organic matter flux and planktonic new production in the deep ocean, *Nature, 282*, 677-680, 1979.

Fairbanks, R. G., M. Sverdlove, R. Free, P. H. Wiebe, and A. W. H. Bé, Vertical distribution and isotopic fractionation of living planktonic foraminifera from the Panama Basin, *Nature, 298*, 841-844, 1982.

Farrell, J. W., and W. L. Prell, Climatic change and $CaCO_3$ preservation: An 800,000 year bathymetric reconstruction from the central equatorial Pacific Ocean, *Paleoceanography, 4*, 447-466, 1989.

Hellermann, S., and M. Rosenstein, Normal monthly wind stress over the world ocean with error estimates, *J. Phys. Oceanogr., 13*, 1093–1104, 1983.

Ingle, S. E., Solubility of calcite in the ocean, *Mar. Chem., 3*, 301-319, 1975.

Jouzel, J., C. Lorius, J. R. Petit, C. Genthon, N. I. Barkov, V. M. Kotlyakov, and V. M. Petrov, Vostok ice core: A continuous isotope temperature record over the last climatic cycle (160,000 years), *Nature, 329*, 403-408, 1987.

Knox, F., and M. B. McElroy, Changes in atmospheric CO_2: Influence of the marine biota at high latitude, *J. Geophys. Res., 89*, 4629-4637, 1984.

Kroopnick, P. M., The distribution of ^{13}C of $\sum CO_2$ in the world oceans, *Deep-Sea Res., 32*, 57-84, 1985.

Levitus, S., Climatological Atlas of the World Ocean, *NOAA Prof. Pap. 13*, Natl. Oceanic and Atmos. Admin., Rockville Md., 1982.

Li, Y. H., T. Takahashi, and W. S. Broecker, Degree of saturation of $CaCO_3$ in the oceans, *J. Geophys. Res., 74*, 5507-5525, 1969.

Longhurst, A. R., and W. G. Harrison, Vertical nitrogen flux from the oceanic photic zone by diel migrant zooplankton and nekton, *Deep-Sea Res., 35*, 881-889, 1988.

Lorius, C., J. Jouzel, C. Ritz, L. Merlivat, N. I. Barkov, Y. S. Korotkevich, and V. M. Kotlyakov, A 150,000-year climatic record from Antarctic ice, *Nature, 316*, 591-596, 1985.

Maier-Reimer, E., and K. Hasselmann, Transport and storage of CO_2 in the ocean - an inorganic ocean-circulation carbon cycle model, *Clim. Dyn., 2*, 63-90, 1987.

Maier-Reimer, E., and R. Bacastow, Modelling of geochemical tracers in the ocean, in *Climate-Ocean Interaction*, edited by M. E. Schlesinger, pp. 233-267, Kluwer Acad. Publ., Dordrecht, 1990.

Marotzke, J., P. Welander, and J. Willebrand, Instability and multiple steady states in a meridional-plane model of the thermohaline circulation, *Tellus, 40A*, 162-172, 1988.

Martinson, D. G., N. G. Pisias, J. D. Hays, J. Imbrie, T. D. Moore, Jr., and N. J. Shackleton, Age dating and orbital theory of the ice ages: Development of a high-resolution 0 to 300,000-year chronostratigraphy, *Quat. Res., 27*, 1-29, 1987.

Mehrbach, C., C. H. Culberson, J. E. Hawley, and R. M. Pytkowicz, Measurement of the apparent dissociation constants of carbonic acid in seawater at atmospheric pressure, *Limnol. Oceanogr., 18*, 897-907, 1973.

Minster, J.-F., and M. Boulahdid, Redfield ratios along isopycnal surfaces - A complementary study, *Deep-Sea Res., 34*, 1981-2004, 1987.

Neftel, A., H. Oeschger, J. Schwander, B.Stauffer, and R. Zumbrunn, Ice core sample measurements give atmospheric CO_2 content during the past 40,000 yr, *Nature, 295*, 220-223, 1982.

Oeschger, H., B. Stauffer, R. Finkel, and C. C. Langway, Jr., Variations of the CO_2 concentration of occluded air and of anions and dust in polar ice cores, in *The Carbon Cycle and Atmospheric CO_2: Natural Variations Archean to Present*, Geophys. Monogr. Ser. vol. 32, edited by E. T. Sundquist, and W. S. Broecker, pp. 132-142, AGU, Washington, D. C., 1985.

Oudot, C., C. Andrie, and Y. Montel, Evolution du CO_2 océanique et atmosphérique sur la période 1982-1984 dans l'Atlantique tropical, *Deep-Sea Res., 34*, 1107-1137, 1987.

Packard, T. T., M. Denis, M. Rodier, and P. Garfield, Deep-ocean metabolic CO_2 production: calculations from ETS activity, *Deep-Sea Res., 35*, 371-382, 1988.

Parsons, T. R., and M. Takahashi, *Biological Oceanographic Processes,* 186 pp., Pergamon, New York, 1973.

Peng, T.-H., and W. S. Broecker, C/P ratios in marine detritus, *Global Biogeochem. Cycles, 1*, 155-161, 1987.

Peterson, L. C., and W. L. Prell, Carbonate preservation and rates of climatic change: An 800 kyr record from the Indian Ocean, in *The Carbon Cycle and Atmospheric CO_2: Natural Variations Archean to Present*, Geophys. Monogr. Ser. vol. 32, edited by E. T. Sundquist, and W. S. Broecker, pp. 251-269, AGU, Washington, D. C., 1985.

Romankevich, E. A., *Geochemistry of Organic Matter,* 334 pp., Springer-Verlag, New York, 1984.

Rooth, C., Hydrology and ocean circulation, *Progr. Oceanogr., 11*, 131-149, 1982.

Sarmiento, J. L., and J. R. Toggweiler, A new model for the role of the oceans in determining atmospheric pCO_2, *Nature, 308*, 620-624, 1984.

Sarnthein, M., H. Erlenkeuser, R. von Grafenstein und C. Schröder, Stable-isotope stratigraphy for the last 750,000 years: "Meteor" core 13519 from the eastern equatorial Atlantic, *Meteor Forschungsergeb., Reihe C, 38*, 9-24, 1984.

Sarnthein, M., K. Winn, J.-C. Duplessy, and M. Fontugne, Global variations of surface

ocean productivity in low and mid latitudes: Influence on CO_2 reservoirs of the deep ocean and atmosphere during the last 21,000 years, *Paleoceanography, 3*, 361-399, 1988.

Shackleton, N. J., Carbon-13 in Uvigerina: Tropical rainforest history and the equatorial Pacific carbonate dissolution cycles, in *The Fate of Fossil Fuel CO_2 in the Oceans*, edited by N. R. Andersen and A. Malahoff, pp. 401-427, Plenum, New York, 1977.

Shackleton, N. J., and N. G. Pisias, Atmospheric carbon dioxide, orbital forcing, and climate, in *The Carbon Cycle and Atmospheric CO_2: Natural Variations Archean to Present*, Geophys. Monogr. Ser. vol. 32, edited by E. T. Sundquist, and W. S. Broecker, pp. 303-317, AGU, Washington, D. C., 1985.

Shackleton, N. J., J. Imbrie, and M. A. Hall, Oxygen and carbon isotope record of East Pacific core V19-30: Implications for the formation of deep water in the late Pleistocene North Atlantic, *Earth Planet. Sci. Lett., 65*, 233-244, 1983.

Shackleton, N. J., J.-C. Duplessy, M. Arnold, P. Maurice, M. A. Hall, and J. Cartlidge, Radiocarbon age of last glacial Pacific deep water, *Nature, 335*, 708-711, 1988.

Siegenthaler, U., and T. Wenk, Rapid atmospheric CO_2 variations and ocean circulation, *Nature, 308*, 624-626, 1984.

Stommel, H., Thermohaline convection with two stable regimes of flow, *Tellus, 13*, 224-230, 1961.

Suess, E., Particulate organic carbon flux in the oceans - Surface productivity and oxygen utilization, *Nature, 288*, 260-263, 1980.

Takahashi, T., W. S. Broecker, and S. Langer, Redfield ratio based on chemical data from isopycnal surfaces, *J. Geophy. Res., 90*, 6907-6924, 1985.

Weiss, R. F., The solubility of nitrogen, oxygen and argon in water and seawater, *Deep-Sea Res., 17*, 721-735, 1970.

Weiss, R. F., Carbon dioxide in water and sea water: The solubility of a non-ideal gas, *Mar. Chem., 2*, 203-215, 1974.

Weiss, R. F., H. G. Östlund, and H. Craig, Geochemical studies of the Weddell Sea, *Deep-Sea Res., 26, 1093-1120, 1979.*

Woodruff, S. D., R. J. Slutz, R. L. Jenne, and P. M. Steurer, A comprehensive ocean-atmosphere data set, *Bull. Am. Meteorol. Soc., 68*, 1239-1250, 1987.

Zahn, R., K. Winn, and M. Sarnthein, Benthic foraminiferal $\delta^{13}C$ and accumulation rates of organic carbon: Uvigerina peregrina group and Cibicidoides wuellerstorfi, *Paleoceanography, 1*, 27-42, 1986.

C. Heinze, Institut für Meereskunde der Universität Hamburg, Troplowitzstraße 7, D-2000 Hamburg 54, Federal Republic of Germany.

E. Maier-Reimer, Max-Planck-Institut für Meteorologie, Bundesstraße 55, D-2000 Hamburg 13, Federal Republic of Germany.

K. Winn, Geologisch-Paläontologisches Institut und Museum der Christian-Albrechts-Universität, Olshausenstraße 40, D-2300 Kiel 1, Federal Republic of Germany.

(Received July 24, 1990;
revised February 8, 1991;
accepted February 13, 1991.)